UCRL-8664



UNIVERSITY OF CALIFORNIA

Lawrence Radiation Laboratory
Berkeley, California

Contract No. W-7405-eng-48

# NUCLEAR DECAY SCHEME STUDIES OF SOME TANTALUM AND TERBIUM ISOTOPES

Kenneth T. Faler
(Thesis)

April 1959

Printed for the U. S. Atomic Energy Commission

## DISCLAIMER

Printed in USA. Price $2.25. Available from the
Office of Technical Services
U. S. Department of Commerce
Washington 25, D. C.

NUCLEAR DECAY SCHEME STUDIES OF SOME TANTALUM AND TERBIUM ISOTOPES

Contents

# NUCLEAR DECAY SCHEME STUDIES OF SOME TANTALUM AND TERBIUM ISOTOPES

Kenneth T. Faler

Lawrence Radiation Laboratory and Department of Chemistry
University of California, Berkeley, California

April 1959

## ABSTRACT

A previously unreported isotope of terbium, $Tb^{152}$, was produced. Its gamma-ray spectrum was studied and its half life was determined to be 18.5±0.5 hr. The similarity to the half lives of two neighboring isotopes, 19-hr $Tb^{151}$ and 17-hr $Tb^{154}$, explains why it was previously overlooked.

The decay scheme of $Tb^{161}$ was studied and precise transition energies are reported. The lifetimes of two excited states were measured and used to resolve a question of transition sequence encountered by previous investigators.

Three new isotopes of tantalum were discovered. They are 3.7-hr $Ta^{173}$, 1.2-hr $Ta^{174}$, and 11-hr $Ta^{175}$. Tantalum-175 was studied in detail and a decay scheme is presented using eight of the transitions observed in conversion-electron studies. Four excited states are proposed, and Nilsson quantum numbers are assigned.

Electron-sensitive nuclear track emulsions were used in conjunction with electron spectrographs, and the usefulness of the method of track counting is discussed.

# NUCLEAR DECAY SCHEME STUDIES OF SOME TANTALUM AND TERBIUM ISOTOPES

Kenneth T. Faler

Lawrence Radiation Laboratory and Department of Chemistry
University of California, Berkeley, California

April 1959

## I. INTRODUCTION

The great success of a model based on the collective motion of nucleons in predicting nuclear properties, and particularly rotational energy-level spacings, has stimulated wide interest in the regions of nuclides to which the model applies. These are, first, the heavy-element region above the closed shells at Z = 82 and N = 126, and, second, in the region of rare earths and neighboring elements between closed shells at N = 82 and N = 126. A further stimulus to detailed investigation of nuclear energy levels in these regions is the possibility of a systematic description of the observed intrinsic states on the basis of wave functions in a deformed potential. It is of great interest to search for and identify the states involved, permitting a comparison to be made with the theoretical predictions. A set of quantum numbers is thus assigned to each observed state, allowing it to be characterized throughout the region in which it appears.

Chemical separation of rare earth elements by highly refined ion-exchange techniques has enabled nuclear chemists to study the properties of their isotopes extensively. Even so, a great deal of information remains to be obtained by conventional methods. In this study two isotopes of terbium were made by 60-inch cyclotron bombardments, and their properties were characterized. Of these two, $Tb^{152}$ had been previously unreported.

The completion of the heavy-ion linear accelerator has made possible the production of many neutron-deficient nuclides which were previously difficult to make. The light isotopes of tantalum were the object of one section of the study.

Finally, the constant effort to improve the methods by which decay schemes are investigated has led to an attempted improvement in the sensitivity and ability to measure relative intensities of one of the more useful instruments in use at this laboratory, the permanent-magnet electron spectrograph. Electron-sensitive nuclear emulsions were substituted for ordinary spectrograph plates, and the tracks produced by conversion electrons were counted individually under a microscope. The range of usefulness and degree of improvement obtained have been determined.

## II. EXPERIMENTAL METHODS

### A. Bombardment Procedure

The isotopes produced in these studies were made by nuclear reactions using lanthanide elements in their oxide powder form as targets. Lutetium and holmium oxides were obtained as commercially purified compounds. Two stable separated isotopes were obtained from Oak Ridge. These were 95.4% $Gd^{160}$ with 3.1% $Gd^{158}$, and 91.9% $Eu^{151}$ with 8.1% $Eu^{153}$.

Alpha-particle bombardments were carried out on the Berkeley 60-inch cyclotron, and nitrogen-ion bombardments on the Berkeley heavy-ion linear accelerator. Target material for both accelerators was prepared by placing a slurry of the oxide powder in Duco cement diluted with amyl acetate on platinum plates having indentations suitable for the size of the sample and shape of the beam pattern. The organic material was burned off, before bombardment of cyclotron targets or after bombardment of heavy-ion targets, by holding the sample and plate in a bunsen burner flame. The sample was covered with aluminum or platinum foil, which served to hold the powder in the cup and also to degrade the bombarding particles to the energy desired for the particular reaction. These plates and foil assemblies were mounted in standard target blocks designed for cooling and positioning the target.

Thermal-neutron reactions were carried out in the Materials Testing Reactor at Arco, Idaho. Samples for these irradiations were sealed in quartz tubes 6 millimeters in outside diameter and about 1-1/4 inches long. These tubes were placed inside screw-cap aluminum containers for irradiation in standard sample holders used at the reactor.

### B. Chemistry

Terbium was separated from the other lanthanide elements by means of ion-exchange techniques. The bombardment sample of 1 milligram or less was dissolved by adding a few drops of 12 N HCl to the powder in the sample-plate indentation. The material dissolved readily with gentle heating and the solution was evaporated to dryness. The chloride was redissolved in a minimum of 0.05 N HCl and transferred to the ion-exchange

column. This column was 0.3 cm in diameter and about 8 cm long and had a free column volume of 10 drops. The resin was Dowex-50 200-to-400-mesh, 12% cross-linked, and the column was enclosed in a heating jacket kept at 82°C by isopropyl alcohol vapor. Elution was carried out according to a method described elsewhere[1] with 0.4 M alpha-hydroxyisobutyric acid buffered to pH 4.0. The isobutyrate was removed by acidifying the eluting solution to about 0.1 N and adsorbing the terbium onto 4% cross-linked Dowex-50 resin in a small column about 0.5 cm in length. Following thorough washing with dilute acid the activity was eluted with 8 N HCl.

Separation of tantalum was based on a method described by Stevenson and Hicks.[2] The lanthanide is dissolved as above and transferred into a polyethylene cone. About 0.2 mg of tungsten fluoride carrier is added, and the lanthanum fluorides are precipitated with HF and are removed for recovery. The concentrations are adjusted to 6 N HCl and 2 N HF, and the tantalum is extracted into di-isopropyl ketone. Tantalum is back-extracted into distilled water containing a drop of saturated $H_3BO_3$ solution which has been added to complex the fluoride ions.

C. Source Preparation

The activity was prepared for Geiger counting or gamma-ray scintillation counting by evaporating either a portion of the final water solution or some of the di-isopropyl ketone solution or the isobutyrate eluant on aluminum plates. These plates were placed on cardboard sample holders and were usually covered with a strip of transparent Scotch tape. Samples for alpha-particle counting were prepared from the final water solution by evaporating to dryness on platinum plates and flaming in a bunsen burner.

Spectrometer samples were evaporated to dryness on aluminum strips welded to standard sample-holder rings. Permanent-magnet spectrograph samples were made by using an electrodeposition technique due to Harvey[3] in which the hydroxide of the metal is plated out onto a 10-mil

platinum wire from a buffered plating solution. This solution was 0.1 M ammonium bisulfate at pH 3.6 for the terbium and about 40 mg per ml of ammonium oxalate for tantalum. The plating procedure has previously been described in detail.[4]

D. Instruments

Decay rates of gross activity were followed by counting samples with ordinary mica end-window Geiger-Mueller counters. Gamma spectra were studied on a 100-channel pulse-height analyzer[5] used with a 3-by-3-inch NaI(Tl) scintillation crystal, photomultiplier tube, and associated electronic components. Gamma-gamma coincidence determinations were also made with this instrument in conjunction with a single-channel analyzer and using two crystals 1 in. in diameter by 1-1/2 in. high.

Gamma-ray lifetimes were measured by the method of delayed coincidences on apparatus described by Juliano.[6]

Alpha particles were counted in an argon gas-flow ionization chamber with 100% counting efficiency and 51% geometry. Alpha-particle measurements were also made on a gas-flow counter coupled with a 50-channel pulse-height analyzer.[7]

Conversion-electron spectra were studied by means of a double-focusing electron spectrometer[8] and a series of four permanent-magnet electron spectrographs with field strengths of 52, 99, 214, and 340 gauss.[4]

The microscope used in electron-track counting was a Bausch and Lomb model TBR-8. Eyepieces were Leitz 12X B periplan lenses with a 6-by-6 grid reticle. Objective lenses included a Bausch and Lomb 43X dry and a 90X Spencer apochromat oil-immersion. The microscope stage was screw-operated in both the X and Y directions, with micrometer wheel and vernier scales giving position readings to one micron. Positioning in the X direction was reproducible to ± 2 microns. A variable-intensity light source, "Ortho-Illuminator B," was obtained from Silge and Kuhne of San Francisco and was modified slightly as to angle of emitted light.

E. Intensity Measurements

The relative intensities of gamma rays in a pulse-height spectrum were obtained by subtracting pulse-height distributions of single gamma-ray standards from the complex spectrum in steps, starting with the highest-energy photopeak seen. Efficiency corrections were made according to data taken from Heath.[9] Escape-peak corrections were made on the basis of curves given by Axel.[10] Decay rates of single gamma rays were obtained by integrating successive photopeak areas above the observed peak height at half maximum or some multiple of half maximum.

Relative intensities of conversion electrons were obtained when possible by integration of peak areas in spectrometer spectra. Closely spaced lines and lines of low relative intensity were compared with standard spectrograph plates of known line darkness. Densitometer tracings were made to measure relative exposure.[4] A visual comparison method was also utilized in which plates of known exposure times were used as standards.[11]

Development of an electron-track method is described in Section VI. In this method electron-spectrograph plates with Ilford G5 emulsion layers 25 microns thick were used. These plates were developed for 1 hour in Kodak D-19 developer diluted to 1/6 of the recommended strength. Plates were fixed in full-strength Kodak acid fix for 15 minutes, washed, soaked in 5% glycerine, and air-dried. Counting was done by choosing a region a few millimeters long and making counts at randomly selected microscope stage settings. Previous counting results were covered before each new count. Both of these latter steps were taken to avoid operator bias.

## III. TERBIUM-152

### A. Introduction

Terbium-152 has not been previously reported despite the fact that $Tb^{151}$, $Tb^{153}$, and $Tb^{154}$ have been known for some time. Handley and Lyon[12] studied the neutron-deficient isotopes of terbium and saw no activity with a half life that could be assigned to $Tb^{152}$. They concluded that the half life either was very nearly that of some other isotope in the region or was less than 10 minutes or greater than 5 years. Toth also failed to see activity that could be ascribed to $Tb^{152}$;[13] however, the relative intensities of some of the gamma rays assigned to $Tb^{151}$ seemed to vary outside of experimental error, stimulating further investigation of this isotope.

### B. Results

Comparisons were made between terbium gamma spectra resulting from alpha-particle bombardment of europium using the enriched isotopes, $Eu^{151}$ and $Eu^{153}$, with bombarding energies of 48 Mev and 37 Mev. At the higher energy the most probable reaction is $(\alpha,4n)$, while the lower energy is below the threshold for this reaction and produced mostly $(\alpha,3n)$.

In Fig. 1, Curve A shows the gamma-ray spectrum of the chemically separated terbium isotopes following 37-Mev alpha-particle bombardment of $Eu^{153}$. This sample should consist mostly of $Tb^{154}$ with smaller amounts of $Tb^{155}$ and very little $Tb^{153}$ and $Tb^{152}$. The three peaks have energies (determined precisely by conversion-electron measurements) of 123.2, 248.1, and 347.1 kev, and have hitherto been ascribed to $Tb^{154}$ decay.[14,15]

Curve B of Fig. 1 shows the gamma spectrum following 37-Mev alpha-particle bombardment of $Eu^{151}$. Most of the product should be $Tb^{152}$, with smaller amounts of $Tb^{153}$ and $Tb^{154}$. Again a peak is seen at 340 kev and its rate of decay is obtained from a series of spectra taken at various times after bombardment indicates a half life nearly

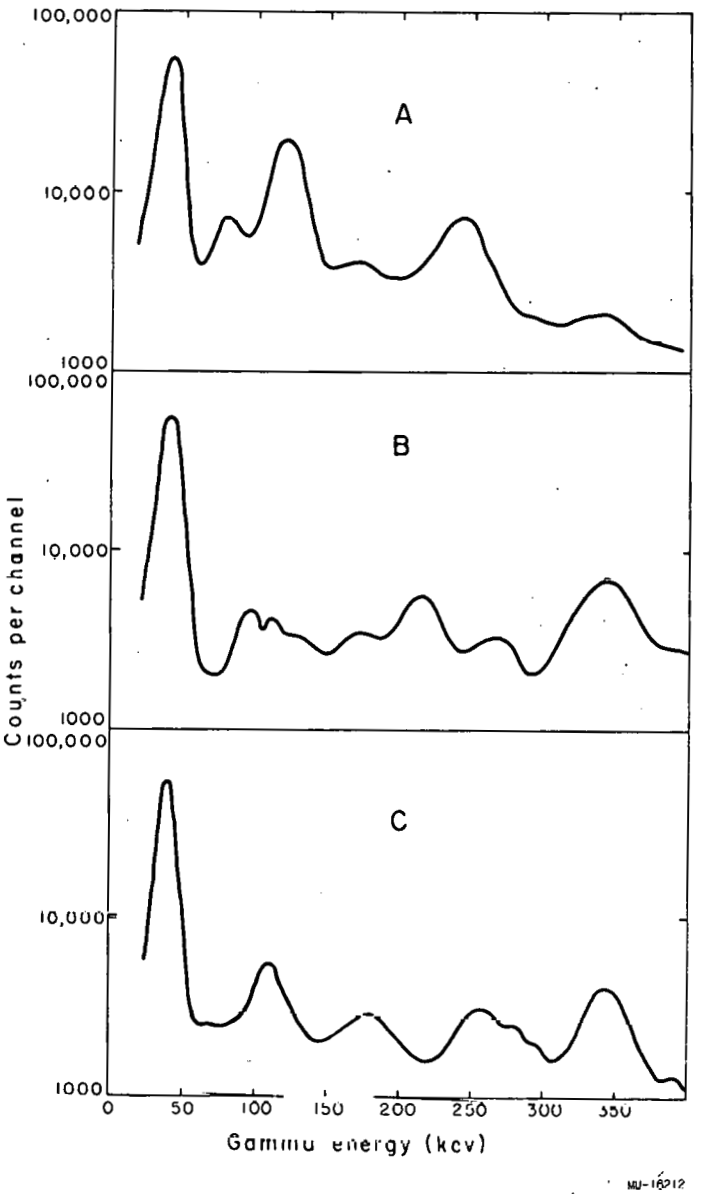


Fig. 1. Gamma-ray spectra of terbium isotopes produced by alpha-particle bombardment of enriched europium isotopes. (A) 37-Mev alphas on $Eu^{153}$, 3x3-inch NaI (Tl) detector; (B) 37-Mev alphas on $Eu^{151}$, 3x3-inch detector; and (C) 48-Mev alphas on $Eu^{151}$, 1.5x1-inch detector.

the same as that of $Tb^{154}$. That it is not, in fact, the same gamma as the 347.1-kev one of $Tb^{154}$ is readily seen when its intensity is compared with the intensities of the other peaks seen in the $Tb^{154}$ spectrum in Curve A. In Curve B the relative intensities of the 120- and 240-kev gammas are greatly reduced. This evidence indicates the presence of an isotope whose decay includes a prominent 340-kev gamma. Since $Tb^{153}$ is known to have a half life of 60 hr,[14] the isotope must be $Tb^{152}$ or perhaps $Tb^{151}$, which also has nearly the same half life. Since this bombardment was at an energy below the threshold for production of $Tb^{151}$ it is most probable that the gamma ray belongs to $Tb^{152}$, and additional evidence is obtained by comparison with Curve C of Fig. 1. This is the spectrum of gamma rays following a 48-Mev bombardment of $Eu^{151}$ which produced an abundance of $Tb^{151}$. This spectrum was obtained with a 1x1-1/2 inch scintillation crystal, therefore in a visual-intensity comparison with the upper curves the different counting efficiencies must be borne in mind. It is possible, however, to obtain relative intensities of gamma rays and correct these for differences in counting efficiencies in order to make comparisons between Curves B and C.[9] This having been done, the corrected intensity ratio of the 340-kev gamma to the 110-kev gamma (even assuming all of the 110-kev peaks in Curves B and C to be due to $Tb^{151}$) is 9.5 to 1 in Curve B and 5.8 to 1 in Curve C. This variation strongly supports assignment of the 340-kev gamma to $Tb^{152}$.

The spectrum shown in Curve B was obtained 32 hours after bombardment, and thus some of the peaks shown are due to gamma rays of longer-lived nuclides. The peak at 212.2 kev is the prominent gamma seen in the decay of 62-hr $Tb^{153}$. The peaks near 100 kev are complex, consisting of the 97.3- and 103.1-kev gammas from the decay of $Gd^{153}$ and several weak gammas from $Tb^{153}$ decay. No gamma rays are seen that can be assigned to $Tb^{151}$ or $Tb^{154}$. A spectrum taken at higher energies shows a large number of low-intensity gammas which could not be resolved and assigned with certainty. From the high-energy side of the 340-kev peak may be resolved a gamma of 415 kev energy with an intensity about 20% that of the 340. This is doubtless the 413-kev gamma ray seen in the decay of $Eu^{152}$ to the same daughter nuclide.

Several sources for the permanent-magnet spectrograph have been made[13] from the terbium fraction of the sample obtained in the 48-Mev alpha-particle bombardment of $Eu^{151}$. Conversion-electron energies were compared with energies observed in the decay of $Eu^{152}$ on the same instrument, and corresponded exactly to those of the 344.1-kev gamma seen here and elsewhere.

In addition to the two gamma rays discussed above, there are peaks at 180 and 265 kev in spectrum B which decayed with about the correct half life to indicate that they belonged to $Tb^{152}$ decay, and there was some indication that a gamma around 90 kev also had a 19-hour half life, but this was less certain. An additional gamma was seen at 125 kev which decayed very rapidly and whose identity or half life was not determined.

Finally, alpha particles from the $Tb^{152}$ decay were sought in the sample obtained from the 37-Mev bombardment of $Eu^{151}$. No alpha counts were detected, and estimating the disintegration rate of $Tb^{152}$ from the K x-ray peak together with the statistical uncertainty in the alpha counter background allowed setting of an alpha-to-electron-capture branching ratio limit as $< 10^{-7}$.

This number is to be compared with the branching ratio of $3 \times 10^{-6}$ for $Tb^{151}$, which has been recently determined experimentally by Toth.[13]

The half life of $Tb^{152}$ was determined by following the decay of the gross activity and by following the decay of the 344-kev peak. It was found to be 18.5±0.5 hr. The similarity of the half lives of two neighboring isotopes, $Tb^{151}$ (19-hr) and $Tb^{154}$ (17-hr) makes it clear why this isotope has been previously overlooked.

# IV. TERBIUM-161

## A. Introduction

Several investigators have studied the decay of 7-day $Tb^{161}$ to states in $Dy^{161}$.[16] In 1956 the results of extensive electron-spectrometer studies were published by Cork et al.[17] and by Smith et al.[18] Both found 25.6- and 48.9-kev transitions in cascade and observed the 74.6-kev crossover, but their decay schemes differed in the assignment of the first excited state. The assignment is based on the relative intensities of the 25.6- and 48.9-kev transitions, the most intense being assumed to proceed to ground. Since the relative intensities are about equal and because it is very difficult to make accurate measurements at the low energies involved, it is not surprising that their results led to different conclusions.

The study reported here was undertaken in order to obtain accurate transition-energy data and to distinguish between the two suggested decay schemes. Conversion-electron data were obtained from permanent-magnet spectrograph plates, and the lifetimes of two excited states were measured in order to resolve the question of the decay sequence.

## B. Conversion-Electron Study

Spectrograph plates were obtained from exposures in the 52-gauss spectrograph, and energies of the conversion-electron lines as computed on the IBM 650 computer are shown in Table I. A small trace of $Tb^{160}$ in the sample served as a convenient energy standard, since it has a transition which has been measured on crystal spectrometers as 86.7 kev. The energy determined by means of the field calibration used in this study was 86.65 kev. Relative intensities are given in terms of s - (strong), m - (moderate), and w - (weak), with v meaning "very"; i.e., vw indicates a very weak line.

Table II compares transition-energy sums and crossover energies of the seven transitions seen in the study. These data are in agreement with those of both Smith et al. and Cork et al. except for one case; the latter reported the $L_I$ line of a 27.7-kev transition which was not seen

Table I

Conversion-electron lines from the decay of $Tb^{161}$

| Electron energy (kev) | Visual intensity | Assignment | Transition energy (kev) |
|---|---|---|---|
| 16.62 | M | $L_I$ | 25.67 |
| 17.11 | M | $L_{II}$ | 25.70 |
| 17.89 | MS | $L_{III}$ | 25.69 |
| 23.59 | MS | $M_I$ [a] | 25.63 |
| 23.75 | W | $M_{II}$ | 25.60 |
| 23.95 | M | $M_{III}$ | 25.63 |
| 24.32 | VW | $M_{IV,V}$ | 25.64 |
| 25.29 | W | N | 25.69 |
| | | | 25.66 [b] |
| 39.86 | VVS | $L_I$ | 48.91 |
| 40.30 | VS | $L_{II}$ | 48.89 |
| 41.08 | VS | $L_{III}$ | 48.88 |
| 46.85 | VS | $M_I$ | 48.89 |
| 47.00 | W | $M_{II}$ | 48.85 |
| 47.19 | VW | $M_{III}$ | 48.87 |
| 48.50 | S | N | 48.90 |
| 48.83 | M | O [a] | 48.88 |
| | | | 48.88 |
| 48.13 | S | $L_I$ | 57.18 |
| 48.83 | M | $L_{II}$ [a] | 57.42 |
| 49.35 | MS | $L_{III}$ [a] | 57.15 |
| 55.02 | S | $M_I$ | 57.06 |
| 55.22 | VVW | $M_{II}$ | 57.07 |
| 55.38 | VVW | $M_{III}$ | 57.06 |
| 56.71 | W | N | 57.11 |
| | | | 57.12 |
| 20.81 | MS | K | 74.58 |
| 65.43 | S | $L_I$ | 74.48 |
| 65.88 | M | $L_{II}$ | 74.47 |
| 66.66 | MS | $L_{III}$ | 74.46 |
| 72.37 | W | M | 74.41 |
| 74.12 | VVW | N | 74.50 |
| | | | 74.49 |
| 23.59 | VW | K [a] | 77.36 |
| 68.68 | VW | $L_{II}$ | 77.20 |
| 69.50 | VW | $L_{III}$ | 77.30 |
| | | | 77.25 |
| 48.83 | M | K [a] | 102.66 |
| | | | 102.7 |
| 52.27 | VW | K | 106.04 |
| | | | 106.0 |

a. Lines not completely resolved. b. Weighted average.

in this study, but which fits well in the proposed decay scheme, Fig. 2. One might expect to see the K line of a transition from the proposed 131.6-kev level to ground, but in this study it would have been masked by the $L_{II}$ line of an 86.6-kev transition due to $Tb^{160}$ present as an impurity in the sample.

Table II

Transition-energy sums in $Tb^{161}$ decay
(kev)

| | | | |
|---|---|---|---|
| 25.66 | + | 48.88 | = 74.54 |
| | | Crossover | = 74.49 |
| 77.25 | + | 25.66 | = 102.81 |
| | | Crossover | = 102.7 |
| 57.13 | + | 74.49 | = 131.62 |
| 106.0 | + | 25.66 | = 131.7 |

C. Lifetime Measurements

The transition order of the 25.66- and the 48.88-kev cascade can be established by measuring their decay rates and the decay rate of the 74.49-kev crossover. The transition which goes to ground will come from a state at an energy equal to the energy of the transition, while its precursor will decay from the 74.49-kev state into that state. Thus the half lives of one of the transitions should be identical with that at 74.49-kev, while the other will be different and characteristic of the lower excited state.

Experimentally one compares the delay curve of the gamma ray being studied to the curve of a standard "prompt" photon of the same energy. Standards chosen were the 28-kev K x-rays of $I^{131}$, and 50-kev K x-rays of $Tm^{170}$, and the 71-kev K x-rays of $Hg^{203}$. Mercury-203 x-rays are associated with a transition whose half life is $2.9 \times 10^{-10}$ seconds,

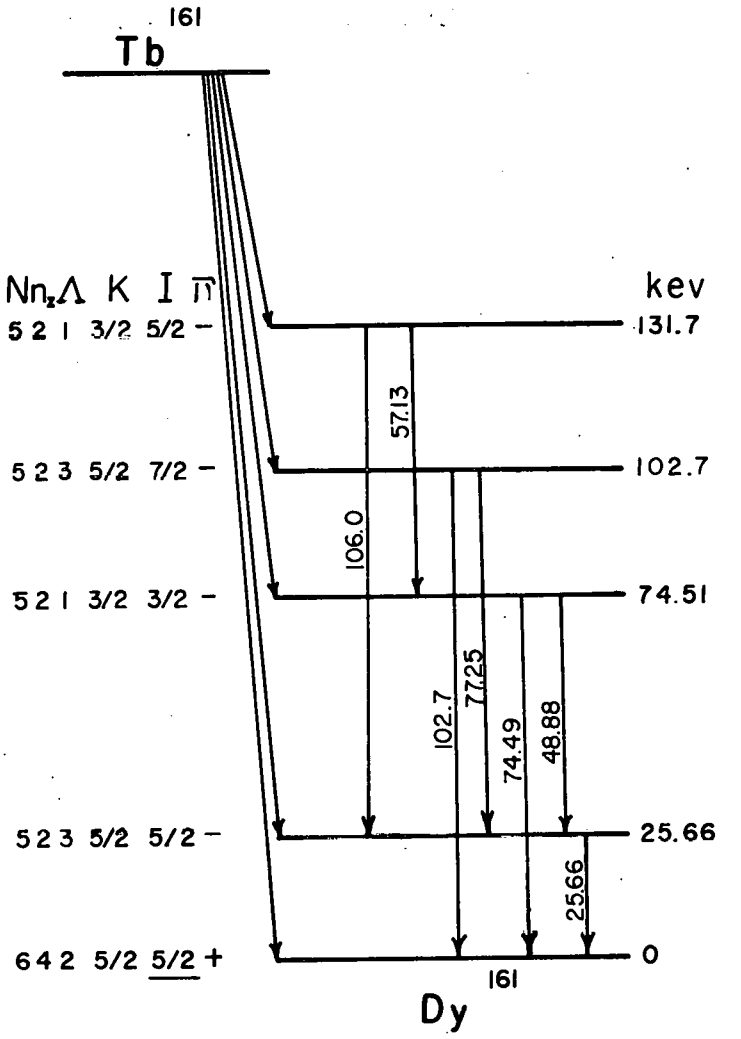


Fig. 2. Decay scheme of $Tb^{161}$.

and a correction must be made for this delay. The other x-ray events are much faster and corrections are negligible. Figure 3 shows the curves obtained from the 25.66-kev transition and its standard. The average of several determinations gave a half life of $29\pm3\times10^{-9}$ sec. Similar curves for the 74.49- and 48.88-kev transitions showed a much shorter half life. The weighted average of several measurements using both the slope of the curve and its centroid shift[6] in the analysis of the data gave $3.1\pm0.6\times10^{-9}$ sec as the half life of the 74.51-kev state. These data agree with the level sequence of Cork in which the first excited state is placed at 25.66 kev, as shown in Fig. 2. From these data the photon-transition half lives of the 25.66- and 48.88-kev transitions are $8.7\times10^{-8}$ sec and $1.1\times10^{-8}$ sec respectively. On the basis of Moszkowski's single-particle half life estimates[19] the photon transitions are delayed by factors of about $1\times10^{4}$ and $1\times10^{2}$ respectively.

D. Recent Work

Subsequent to the study reported above, a number of publications dealing with $Dy^{161}$ levels appeared. McCutchen reported some coincidence and multipolarity studies[20] and reviewed the previous work in detail. He discussed possible intrinsic-state assignments but unfortunately chose the incorrect first excited state given by Smith. A theoretical paper by Bès[21] described the observed levels, as well as others seen in Coulomb excitation and the electron-capture decay of $Ho^{161}$, on the basis of Nilsson's collective-model asymptotic quantum numbers.[22] The ground state has been measured as 5/2,[23] and was assigned as the (642) 5/2+ state according to the notation (N, $n_z$, $\Lambda$) I, $\pi$. The rotational states of this band are not populated sufficiently by beta decay to have been seen in the study reported herein, but have been observed in Coulomb-excitation experiments. The 25.66-kev level was assigned as the (523) 5/2- intrinsic state, with the 102.7-kev state as its 7/2- band member. The 74.49-kev level was also called an intrinsic state, (521) 3/2-, with its 5/2- excited member being the level at 131.7 kev. These assignments are shown in Fig. 3.

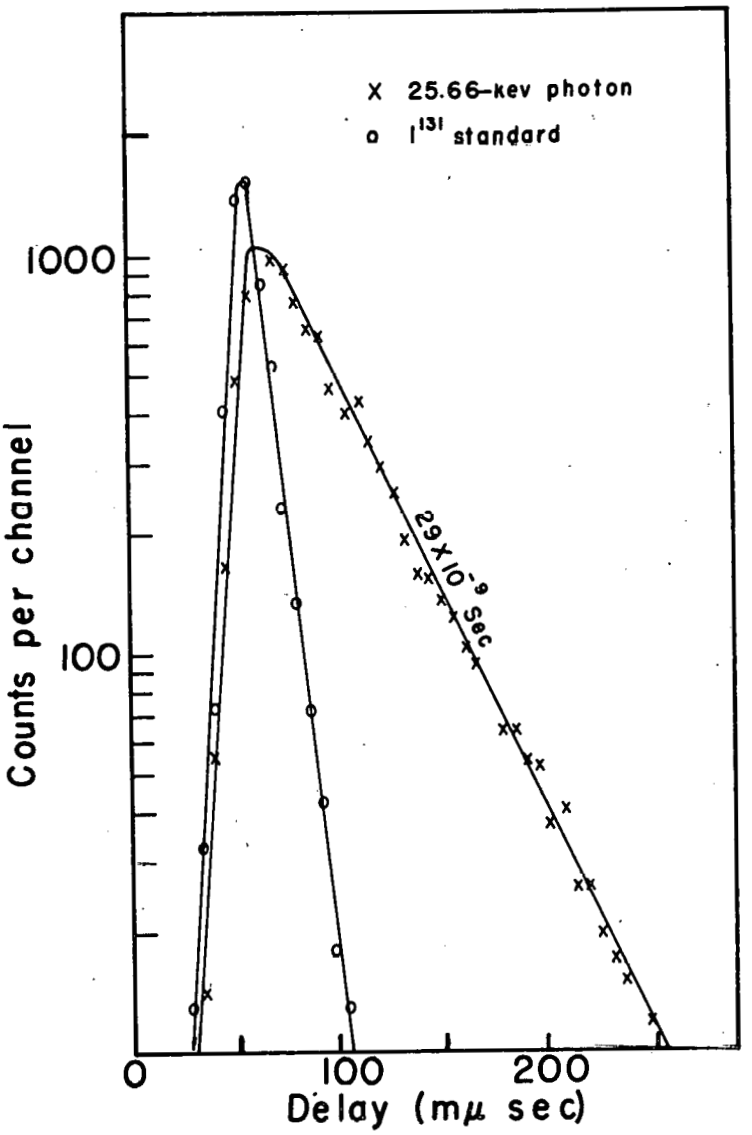


Fig. 3. Coincidence delay curves of the 25.66-kev transition in $Dy^{161}$ and the "prompt" standard.

Hansen et al.[24] reported electron spectrograph work in agreement with that discussed previously and in addition measured the half lives of the same states measured by us. Their results were $28\pm2\times10^{-9}$ sec and $3.0\pm0.3\times10^{-9}$ sec, which agree very well with our values.

A recent Russian publication gave the results of a spectrometer study reporting a very large number of lines. Transitions reported on the basis of these lines included several not seen in previous studies, some of which fit well into the known level sequence. Their suggested state assignments were essentially the same as those previously given, and two additional levels were suggested.

It is interesting to note that three of the intrinsic neutron states in $Dy^{161}$ are the same as the proton states in $Np^{237}$.[22] Since the well-studied 59.6-kev E1 transition in $Np^{237}$, which goes from (523) 5/2- to (642) 5/2+, is analogous to the 25.66-kev E1 transition in $Dy^{161}$ and shows anomolous conversion coefficients, it is of interest to compare the two cases. A theory of anomolous E1 conversion has been presented in a paper by Nilsson and Rasmussen[26] according to which it is expected that the $L_{III}$ coefficient is about normal, while those of the $L_I$ and of the $L_{II}$ are high. The transition rate is retarded and these anomolies appear in several cases of K-allowed transitions which are forbidden by other asymptotic quantum-number selection rules. In the $Np^{237}$ case the $L_{III}$ conversion coefficient is normal, whereas that of the $L_{II}$ is high by 3.8, and the $L_I$ is high by 1.7. Smith et al.[18] have measured the L-subshell ratio of the 25.66-kev $Dy^{161}$ transition and report a value of 1/0.75/1.1. The theoretical value for a pure E1 transition is 1/0.70/1.1, which indicates no anomoly. The transition rate is retarded by a factor of $3\times10^5$ in $Np^{237}$ and of $1\times10^4$ in $Dy^{161}$. This indicates that a difference of 30 in retardation and a change in atomic number from 66 to 93 produces a wide variation in the internal conversion behavior of the two transitions.

The L-subshell ratio has been measured for the 48.88 kev transition also.[17] It is given as about 1/0.16/0.07, while the theoretical value for a pure M1 is 1/0.08/0.02. This ratio does appear

anomalous although a small amount of E2 admixture would improve the agreement somewhat. Since the transition is from the state (521) 3/2- to the state (523) 5/2- it involves a $\Delta \Lambda$ of 2 and a change in nuclear spin direction from parallel to antiparallel with respect to the orbital-angular-momentum vector. The transition is delayed by a factor of only 70. The analogous transition in $Np^{237}$ is delayed by a factor of $1 \times 10^4$ and its conversion coefficient also appears normal.

A third transition common to the two nuclides is the E1 between the (521) 3/2- and the (642) 5/2+ states. This 267-kev transition in $Np^{237}$ is retarded by a factor of $6 \times 10^8$ and its $\alpha_K$ is high by a factor of 10. The transition in $Dy^{161}$ of 74.49 kev energy is retarded by a factor of $1 \times 10^5$. The K/L ratio measured by Hansen is normal and our L-subshell ratio measurement is 2.4/0.6/1, compared with the theoretical value of 2.8/0.8/1 for a pure E1 transition. At this lower atomic number the conversion coefficients appear normal. These comparisons seem to confirm the suggested Z dependence in the anomalous-conversion-coefficient theory.

# V. NEUTRON-DEFICIENT ISOTOPES OF TANTALUM

## A. Introduction

The Berkeley heavy-ion linear accelerator provides a beam of heavy ions with an energy of 10 Mev per nucleon. A beam of these ions -- such as $C^{12}$, $N^{14}$, or $O^{18}$ -- may be used to bombard target material and produce isotopes very difficult to make in relatively pure form by means of other reactions. From the slope of the isotope-stability line one notes that the compound nucleus formed by reaction of the accelerated ion with the target nucleus is already neutron-deficient. At the energies needed to overcome the Coulomb barrier for a given reaction, energy considerations show that the most probable reactions are those involving the emission of several neutrons. Thus bombardment with heavy ions will produce isotopes which are very neutron-deficient and free from isotopes nearer stability. This procedure should allow investigation of short-lived isotopes in the absence of long-lived contamination.

Isotopes of tantalum of mass less than 176 have not been previously reported. These isotopes might be formed by $C^{12}$ bombardment of holmium, but in this case reactions at energies sufficiently above the Coulomb barrier to insure reasonable cross sections would produce only isotopes of mass about 173 and less. For this reason the reaction chosen was $Ho(N^{14},xn)W$. The tungsten isotopes formed are expected to have short half lives and to decay to isotopes of tantalum. The region $Ta^{175}$ and lighter could be investigated by varying the energy of the nitrogen beam, as shown in Table III. In this table the M-A values are computed from Cameron's mass equation.[27] Excitation-function peaks were approximated as being equal to $Q + 2xT$, where Q is the "Q" of the reaction, x the number of emitted neutrons, and T the nuclear temperature, taken as 1.9 Mev.

Since the Coulomb barrier for formation of the compound nucleus $W^{179}$ is 45 Mev, no appreciable amount of $Ta^{176}$ or heavier isotopes should be formed. Thin aluminum foils were used as a convenient method of degrading the beam energy to the desired values. Since there is some uncertainty both in the actual beam energy and in the range-energy relation-

ships for a heavy-ion beam, the energies discussed are those taken from the curve shown in Fig. 4.

Tantalum-175 can also be made by alpha-particle bombardment on the 60-inch cyclotron. The reaction used was $Lu^{175}(\alpha,4n)Ta^{175}$. This reaction should have a high cross section at the full 48-Mev energy available at the cyclotron, and the intense beam produces a large amount of activity, making possible detailed spectrographic studies of the isotope. The reaction also produces large amounts of $Ta^{176}$, but since its conversion-electron lines are well known[30] they may be subtracted out.

Table III

$Ho^{165}(N^{14},xn)W^{A}$ Bombardment energies

| A | M-A (Mev) | x | Threshold (Mev) | Peak (Mev) |
|---|---|---|---|---|
| 179 | 0.709 | 0 | | |
| 178 | -1.016 | 1 | | |
| 177 | -0.436 | 2 | | |
| 176 | -1.767 | 3 | 39 | |
| 175 | -0.766 | 4 | 48 | 60 |
| 174 | -1.679 | 5 | 57 | 72 |
| 173 | -0.214 | 6 | 66 | 84 |
| 172 | -0.638 | 7 | 76 | 97 |
| 171 | 1.303 | 8 | 83 | 107 |
| 170 | 1.373 | 9 | 92 | 119 |

B. Tantalum-173

At bombarding energies of 70 to 110 Mev the presence of $Ta^{173}$ was observed by noting the growth of 124- and 298-kev photopeaks in the gamma-ray spectrum of the tantalum activity. These peaks belong to the daughter nuclide, $Hf^{173}$, and were seen to decay with the 24-hr half life of that nuclide. The decay rate of $Ta^{173}$ was determined from the growth curve of the 298-kev photopeak, as shown in Fig. 5. This is the growth

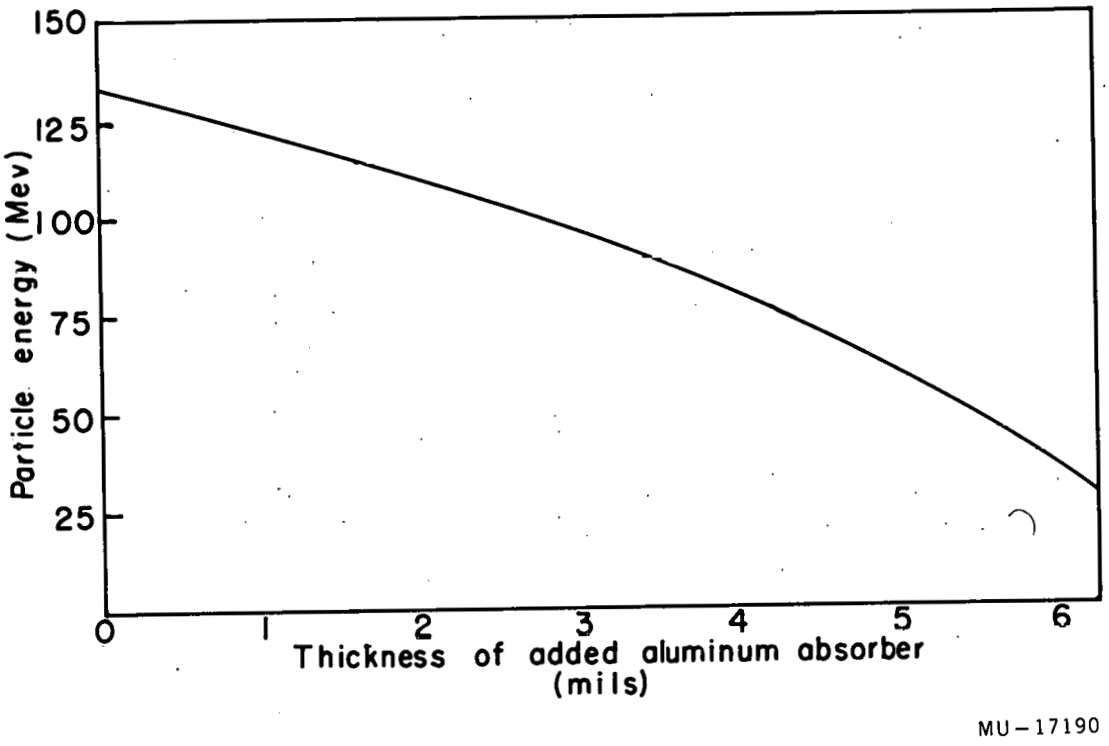


Fig. 4. Energy of $N^{14}$ beam after degradation by aluminum absorbers.

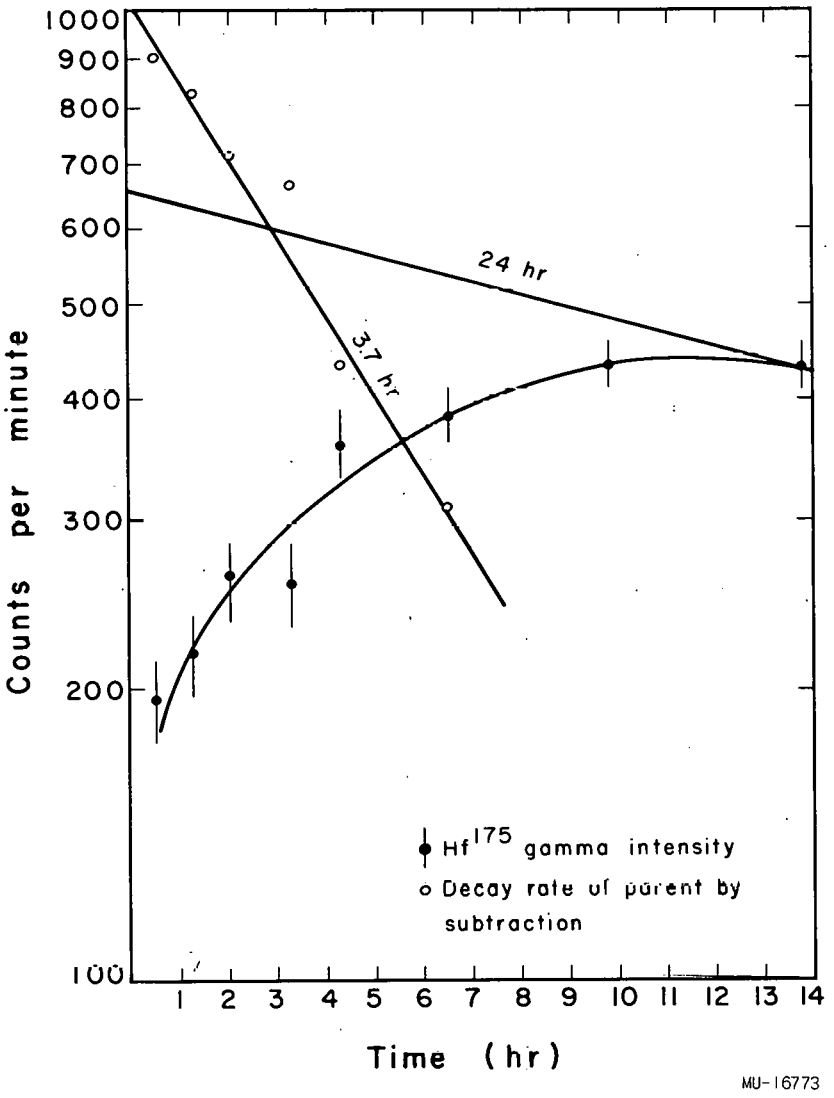


Fig. 5. The half life of $Ta^{173}$ obtained from the growth rate of the 298-kev gamma-ray photopeak of the daughter nuclide, 24-hour $Hf^{173}$.

portion of the curve obtained in a 95-Mev bombardment, and the curves are drawn graphically. For this particular curve, a least-squares fit to the data, performed on the Livermore IBM 704 computer[28] with all points included, gave a value of 4.2±0.7 hr. In this procedure the 24-hr half life of $Hf^{173}$ was held constant while the half life of $Ta^{173}$ and the amounts of activity initially present were varied to give the best fit. A series of determinations from different bombardments gave an average value of 3.7 hr for the half life of $Ta^{173}$.

The gamma-ray spectrum of the tantalum activity produced in the 95-Mev bombardment is shown in Fig. 6. The spectrum is very complex and was not resolved in great detail. Two photopeaks were identified as belonging to $Ta^{173}$ on the basis of their decay rates. They had energies of 90 and 170 kev. Complexity of the spectrum made gamma-gamma coincidence measurements difficult, but results indicated that the two gamma rays were probably in coincidence.

No additional photopeaks were seen in the spectrometer at energies above 500 kev. No additional gamma rays were seen at the highest bombarding energies which were not seen at 70 Mev, and from the time required to accomplish the chemical separation and sample preparation a half-life limit of less than 30 minutes may be set for gamma rays belonging to tantalum isotopes of mass less than 173.

C. Tantalum-174

At bombarding energies of 60 Mev and greater an isotope is formed which decays with a half life of about 1 hour, some of whose gamma rays are shown in Fig. 6. From Table III one expects this isotope to be $Ta^{174}$. Figure 7 shows the gamma-ray spectrum of tantalum following a 70-Mev bombardment. This sample should contain only $Ta^{174}$ and $Ta^{175}$. One notes that the 511-kev annihilation radiation peak is very large relative to that of the K x-rays, indicating a large ratio of positron emission to electron capture for this isotope. Cameron estimates the decay energy of $Ta^{174}$ to be 4.5 Mev and that of $Ta^{173}$ to be 2.8 Mev.[27] If one assumes these values to be approximately correct, the ratio of K-electron capture

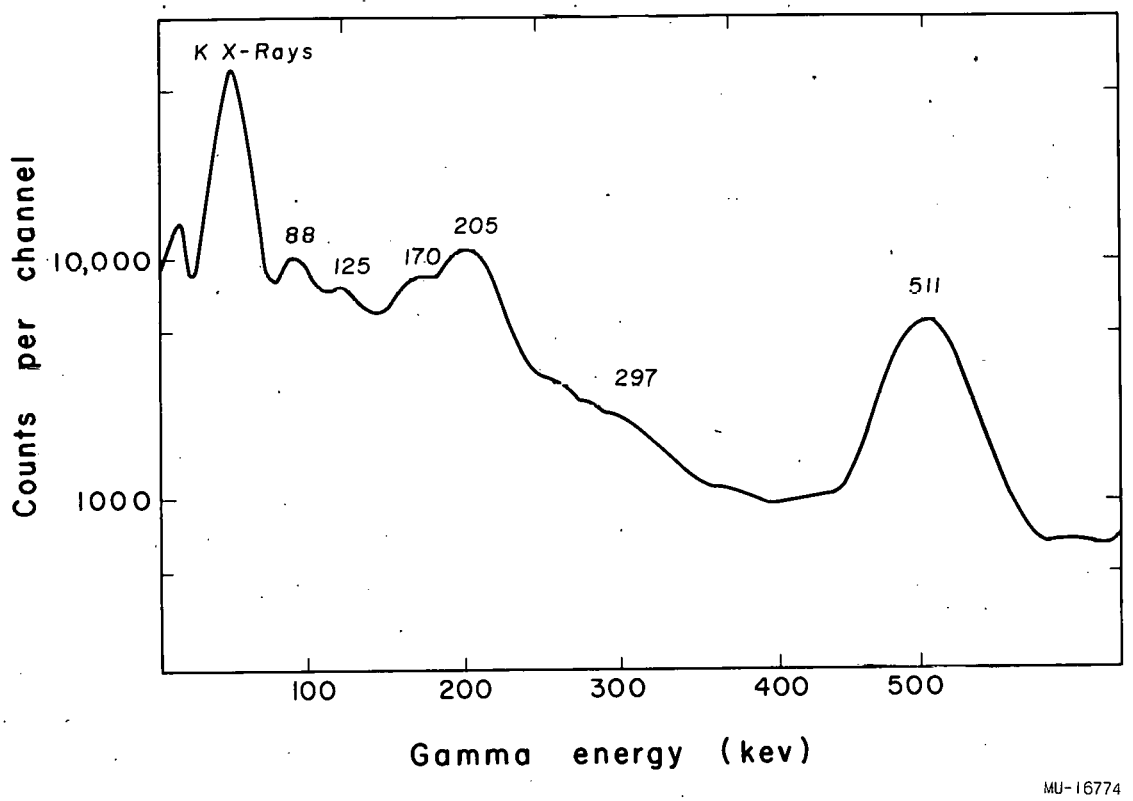


Fig. 6. Gamma-ray pulse-hcight spectrum of $Ta^{173}$ and $Ta^{174}$ produced by $N^{14}$ bombardment of holmium at 95 Mev.

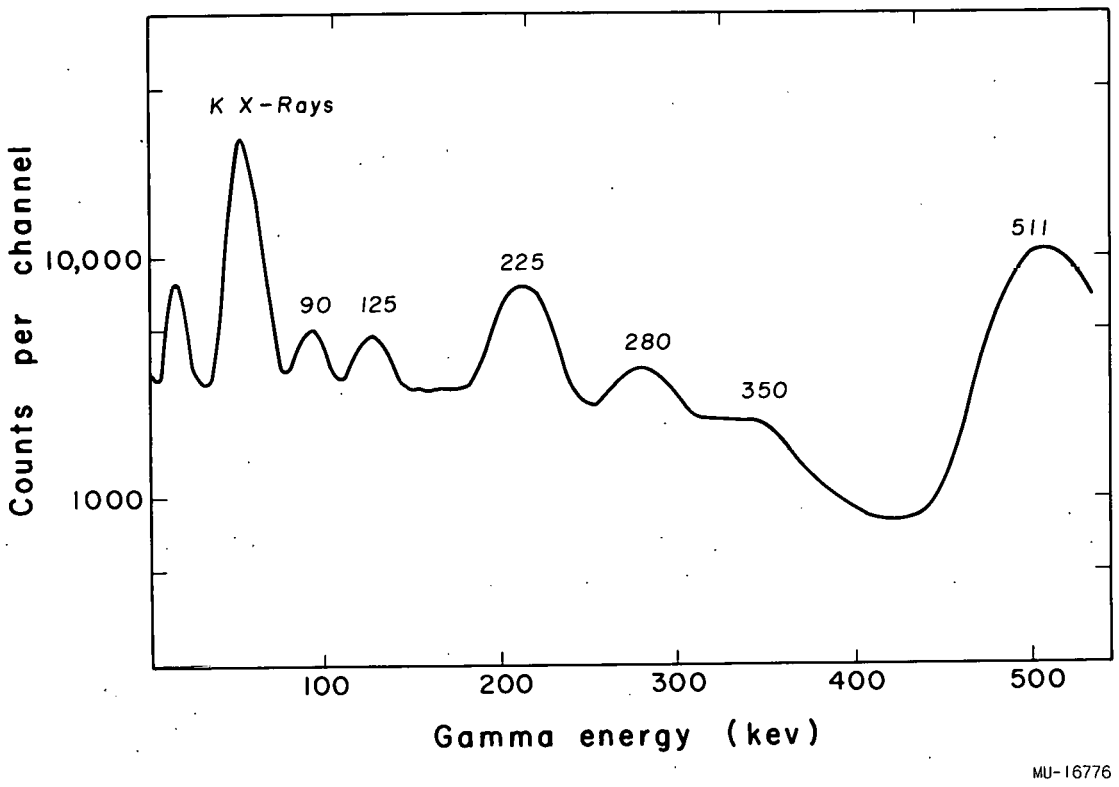


Fig. 7. Gamma-ray pulse-height spectrum of $Ta^{174}$ and $Ta^{175}$ produced by $N^{14}$ bombardment of holmium at 70 Mev.

to positron emission for allowed decay is given by Feenberg and Trigg as 1.6 at 4.5 Mev, and 20 at 2.8 Mev.[29] This is consistent with the mass assignment given for the two isotopes. No activity was seen growing in other than $Hf^{175}$, which is to be expected since $Hf^{174}$ is stable.

Five of the photopeaks in Fig. 7 are assigned to the decay of $Ta^{174}$ on the basis of their decay rates. These are at energies of 90, 125, 205, 280, and 350 kev. In addition there is a peak of lower intensity of 160 kev energy which is clearly seen only in coincidence measurements. The spectrum above 500 kev shows a large number of very-low-intensity peaks which could not be well resolved or confirmed as to half life. Their intensities were less than about 1% of the intensities of the low-energy gamma-ray photopeaks.

The half life of $Ta^{174}$ was determined by following both the decay rate of the gross activity on an end-window G-M counter and the decay rate of the 511-kev photopeak in the gamma-ray spectrum. Figure 8 shows the resolved gross decay curve in which the 11-hr component was subtracted out on the basis of data taken at times longer than those shown in the figure. Figure 9 shows the decay of the 511 kev annihilation radiation photopeak. A series of these determinations led to a measured half life for $Ta^{174}$ of 1.2±0.1 hr.

Gamma-gamma coincidence measurements were made on this spectrum. Gating on the 511-kev photopeak showed that the 90-, 205-, and 160-kev gamma rays were in coincidence with it. Gating on the 205-kev photopeak indicated that the 90- and 280-kev gamma rays were in coincidence with the one at 205 kev.

No gamma rays of more than 1% abundance were detected at energies above 500 kev. Attempts to produce enough of either this isotope or $Ta^{173}$ to study on the conversion-electron spectrometers have not been successful.

D. Tantalum-175

At bombarding energies above 45 Mev an isotope whose half life is 11 hr is formed. This is presumably $Ta^{175}$. Figure 10 is a tantalum gamma-ray spectrum taken 10 hr after a 60-Mev $N^{14}$ bombardment. The time

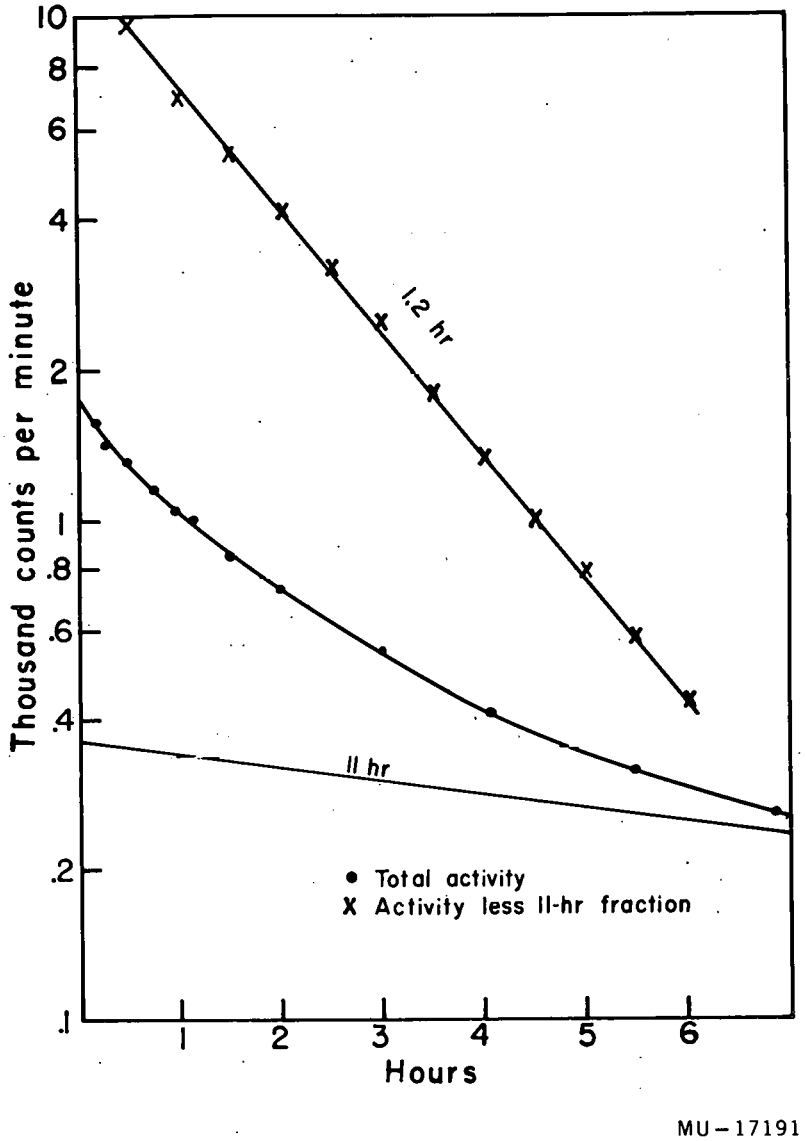


Fig. 8. Decay of $Ta^{174}$ and $Ta^{175}$ gross activity measured by an end-window G-M counter.

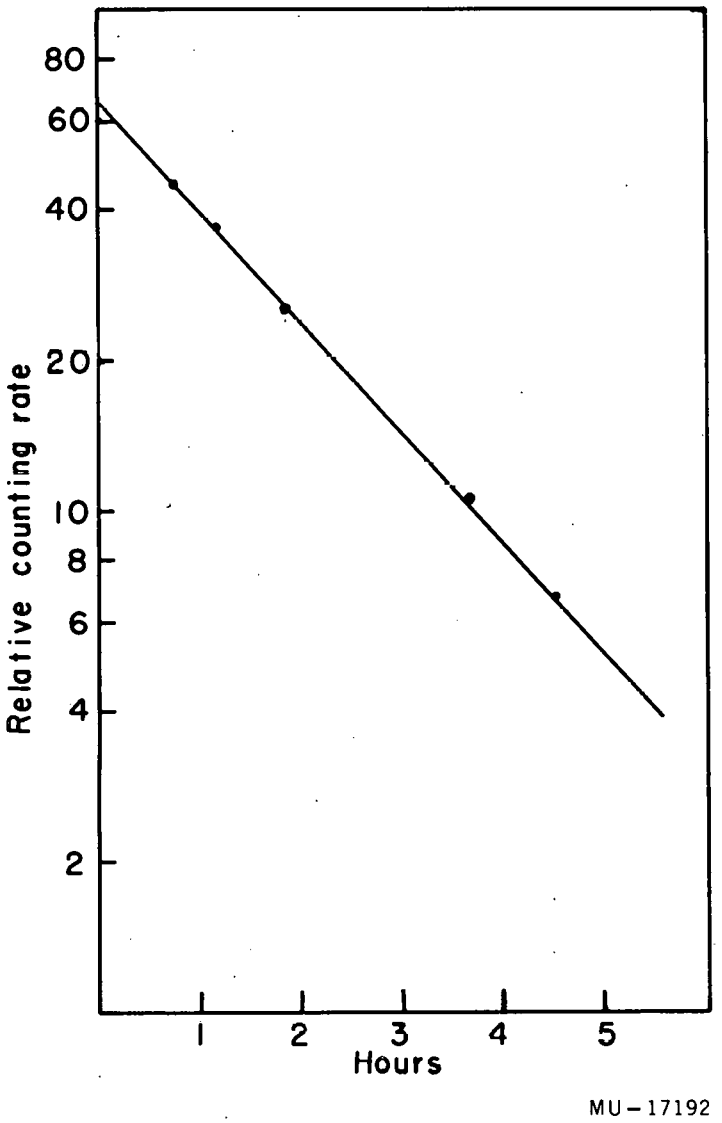


Fig. 9. Decay of the 511-kev photopeak of $Ta^{174}$ obtained from successive gamma-ray spectra.

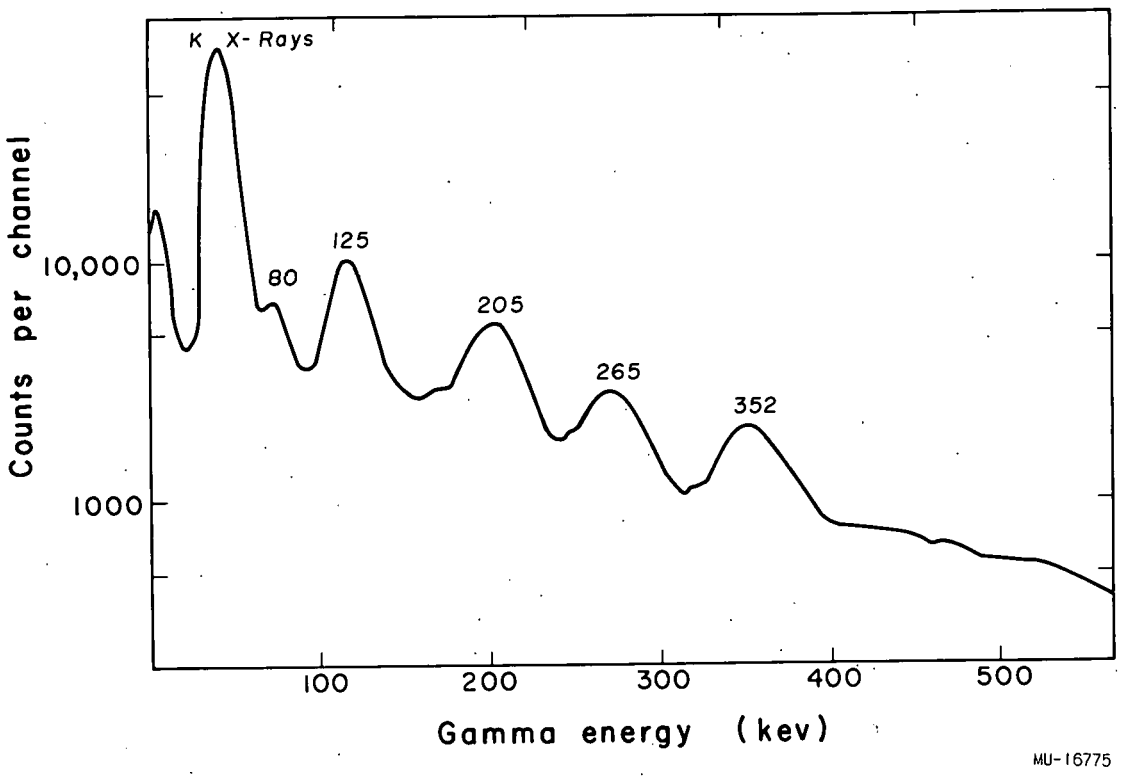


Fig. 10. Gamma-ray pulse-height spectrum of $Ta^{175}$ 10 hours after 60-Mev $N^{14}$ bombardment of holmium.

lapse allowed for the decay of 1.2-hr $Ta^{174}$ also formed in the bombardment. Nearly all the peaks, including the K x-ray peak, have distorted shapes, indicating unresolved components. The 11-hr half life was obtained by following the decay of both the gross activity and the single photopeaks. Since no 511-kev annihilation radiation is observed, a small positron branching ratio and consequently a small decay energy are indicated. This is consistent with the decay energy given by the Cameron mass equation of 1.8 Mev for $Ta^{175}$, which predicts[29] a ratio of K-electron capture to positrons of $1.5 \times 10^3$. Following the decay of this 11-hr isotope, a long-lived activity remains which has a prominent 340-kev gamma ray. This is presumably 70-day $Hf^{175}$, which is the daughter of $Ta^{175}$, and the mass assignment is further confirmed by cross-bombardment with alpha particles.

The maximum energy of the alpha-particle beam of the 60-inch cyclotron is 48 Mev. At this energy the cross section for the reaction $Lu^{175}(\alpha,4n)Ta^{175}$ should be much larger than the cross section for either the $(\alpha,3n)$ or the $(\alpha,5n)$ reaction. Since lutetium is a mixture of 97.4% $Lu^{175}$ and only 2.6% $Lu^{176}$, a full-energy bombardment of natural lutetium should produce a large amount of $Ta^{175}$. The very intense beam of the cyclotron makes the production of enough $Ta^{175}$ for conversion-electron studies relatively easy.

The tantalum gamma-ray spectrum resulting from an alpha-particle bombardment of lutetium is shown in Fig. 11. Comparison with Fig. 10 shows that the photopeaks attributed to $Ta^{175}$ are present. In addition one notes peaks at 88, 113, and 511 kev not seen in Fig. 10. The first two are due to $Ta^{176}$, and the 511-kev peak is from $F^{18}$ not completely removed in the chemical separation. The peak at 405 kev is seen more clearly in this spectrum because of better counting statistics and a contribution from coincidence between the 350-kev photons and K x-rays.

The relative gamma-ray intensities of $Ta^{175}$ were obtained by resolving the spectrum shown in Fig. 10 into its components. The complexity of the spectrum makes the values obtained rather unreliable.

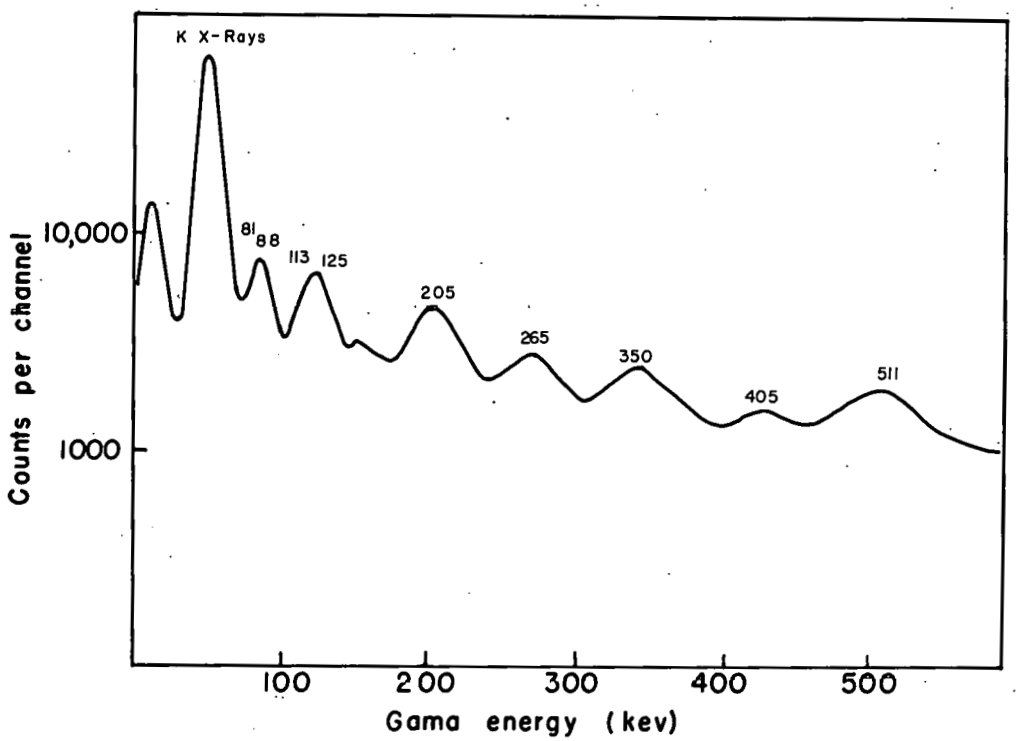


Fig. 11. Gamma-ray pulse-height spectrum of tantalum produced by 48-Mev alpha-particle bombardment of lutetium.

The energies and intensities of gamma rays obtained on resolving the curve are listed in Table IV.

Table IV

The energies given were obtained from conversion-electron data, and the intensities were normalized as discussed below.

| Energy (kev) | Relative intensity |
|---|---|
| 81.6 | < 9 |
| 126.2 | 29.5 |
| 162.5 | 7 |
| 207.9 | 25 |
| 267.2 | 20 |
| 349.0 | 18 |

E. Tantalum-175 Conversion-Electron Spectrum

The conversion-electron spectrum of $Ta^{175}$ produced in the alpha-particle bombardment was studied on three permanent-magnet electron spectrographs. Eighteen transitions were seen and identified by their half lives as belonging to the decay of $Ta^{175}$. The energies of the lines, their assignments, and their transition energies are listed in Table V. The transition-energy "best value" was obtained by a weighted average in which more weight was given to the more intense lines and to areas of best field-strength calibration in the spectrometers. Table VI lists a number of lines that were seen but were too weak to have their half lives determined with certainty. The line at 38.80 kev was assumed to be the K line of a weak 140.9-kev transition, since it fits well into the proposed decay scheme. In addition to those lines listed in the tables, others were seen and identified as belonging to the 88.44- and 202.2-kev transitions in the decay of $Ta^{176}$, [30] and the 113.06-kev transition as belonging to the decay of $Ta^{177}$. The latter has been measured on a crystal spectrometer[31] as having an energy of 112.97, which adds to our confidence in the values of the transition energies given in Tables V and VI.

Table V

Conversion-electron lines from the decay of $Ta^{175}$

| Spectrometer line energy (kev) 99 gauss-214 gauss-340 gauss | Assignment | Gamma energy | Transition energy (best value) |
|---|---|---|---|
| 39.24 | $L_I$ | 50.52 | 50.50 |
| 39.75 | $L_{II}$ | 50.50 | |
| 40.91 | $L_{III}$ | 50.48 | |
| 48.04 | $M_I$ | 50.42 | |
| 48.26 | $M_{II}$ | 50.38 | |
| 48.45 | $M_{III}$ | 50.18 | |
| 50.11 | N | 50.65 | |
| 59.27 | $L_I$ | 70.55 | 70.53 |
| 59.78 | $L_{II}$ | 70.53 | |
| 60.94 | $L_{III}$ | 70.43 | |
| 68.11 | $M_{II}$ | 70.49 | |
| 68.42 | $M_{III}$ | 70.53 | |
| 66.06 | $L_I$ | 77.43 | 77.43 |
| 66.68 | $L_{II}$ | 77.43 | |
| 67.86 | $L_{III}$ | 77.34 | |
| 16.19 | K | 81.56 | 81.57 |
| 70.27 | $L_I$ | 81.55 | |
| 70.83 | $L_{II}$ | 81.58 | |
| 72.01 | $L_{III}$ | 81.58 | |
| 79.44 | M | 81.57 | |
| 81.00 | N | 81.54 | |
| 81.47 | O | 81.55 | |
| 38.80 | K | 104.17 | 104.3 |
| 93.12 | $L_I$ | 104.40 | |
| 93.65 | $L_{II}$ | 104.40 | |
| 94.78 | $L_{III}$ | 104.35 | |
| 60.69 | K | 126.16 | 126.2 |
| 114.84 | $L_I$ | 126.12 | |
| 115.42 | $L_{II}$ | 126.17 | |
| 116.60 | $L_{III}$ | 126.17 | |
| 124.10 | M | 126.21 | |
| 125.75 | N | 126.29 | |
| 91.64 | K | 157.01 | 157.1 |
| 146.38 | L | 157.13 | |
| 97.28 | K | 162.65 | 162.5 |
| 151.55 | L | 162.30 | |

Table V (cont'd.)

| Spectrometer line energy (kev) 99 gauss | 214 gauss | 340 gauss | Assignment | Gamma energy | Transition energy (best value) |
|---|---|---|---|---|---|
| 113.97 | | | K | 179.34 | 179.4 |
| 168.69 | 168.72 | | $L_{II}$ | 179.44 | |
| 169.48 | 169.75 | | $L_{III}$ | 179.05 | |
| | 176.77 | | $M_{II}$ | 179.38 | |
| | 179.06 | | $N_{II}$ | 179.60 | |
| 120.68 | | | K | 186.05 | 186.0 |
| 174.61 | 174.83 | | L | 185.89 | |
| 125.31 | | | K | 190.68 | 190.8 |
| | 179.56 | | L | 190.84 | |
| | 188.24 | | M | 190.85 | |
| 127.73 | | | K | 193.01 | 193.3 |
| | 181.97 | | L | 193.25 | |
| 142.43 | 142.59 | | K | 207.80 | 207.9 |
| 196.43 | 196.60 | | L | 207.71 | |
| 170.13 | | | K | 235.50 | 235.6 |
| | 224.23 | | L | 235.61 | |
| 201.81 | 202.25 | | K | 267.18 | 267.2 |
| | 256.26 | | L | 267.54 | |
| | 265.50 | | M | 268.00 | |
| | 283.53 | 283,63 | K | 348.90 | 349.0 |
| | 338.57 | 338.31 | L | 349.06 | |
| | 346.50 | 346.73 | M | 349.10 | |
| | 328.55 | 328.80 | K | 394.17 | 394.1 |
| | | 383.52 | L | 394.27 | |
| | | 371.86 | K | 437.23 | 437.3 |
| | | 427.15 | L | 437.80 | |

Table VI

Unassigned transitions and electron lines seen in $Ta^{175}$ sample

| Electron energy (kev) | Assignment | Gamma energy | Transition energy (best value) |
|---|---|---|---|
| 222.68 | $L_{II}$[a] | 233.43 | 233.4 |
| 223.89 | $L_{III}$[a] | 233.46 | |
| 165.97 | K | 231.24 | 231.2 |
| 220.45 | L | 231.20 | |
| 229.23 | M | 231.61 | |
| 215.84 | K | 281.22 | 281.2 |
| 269.95 | L | 281.23 | |
| 278.51 | M | 281.12 | |
| 297.62 | K | 362.99 | 363.0 |
| 352.15 | L | 362.90 | |
| 360.58 | M | 362.99 | |
| 402.18 | K | 467.55 | 467.6 |
| 457.01 | L | 476.76 | |
| 419.62 | K | 484.99 | 485.0 |
| 475.49 | L | 485.06 | |
| 482.14 | M | 485.01 | |

Electron lines: 38.80, 55.42, 61.33, 75.58, 110.33, 151.78, 160.43, 164.42, 185.83, 213.38, 321.54, 410.24, 443.16, 448.26, 638.30, 645.93, 883.66, 899.32.

a. Assignment questionable since K line was not seen.

Auger electron lines were quite prominent in the spectrograph plates from the 99-gauss spectrograph. Their energies and assignments are listed in Table VII along with estimated relative intensities.

The relative intensities of the conversion electron lines were determined by three different methods:

A. Integration of peaks obtained on the double-focusing electron spectrometer,

B. densitometer tracing of lines on permanent-magnet spectrograph plates, and

C. visual comparison of spectrograph lines with lines of known exposure.

Since Method A is based on counting numbers of electrons, and since there are no large empirical correction factors between lines except at low energies at which electrons are stopped by the counter window, this method is expected to give the most reliable results. The line of minimum energy whose intensity was measured by this method was the 38.80-kev K line of the 104.33-kev transition. The K line of the 81.57-kev transition was absorbed very strongly by the counter window. The resolution of the instrument is such that the L subshells are not resolved sufficiently to be determined separately, and thus values for the L shell are given as total $L_I + L_{II} + L_{III}$ intensities. A summary of the electron intensities is presented in Table VIII. The L lines of the 70.5-kev transition were not resolved from the K line of the 126.2-kev transition and from a strong unassigned line at 61.33 kev whose visual intensity was 8.1. The total intensity of this group was 39, and is to be compared to the total, obtained by Method C of 43. The K line of the 162.5-kev transition is mixed with the L lines of the 113.06-kev transition of $Ta^{177}$ and only an upper limit can be set for its intensity, although the amount of the contribution from the L lines is expected to be small. Only the stronger lines, which could be resolved and measured accurately, were included in the summary.

Method B involves photographic optical-density measurement of the lines by an integrating densitometer, and is subject to large correction factors due to uncertainties, particularly in the variation of

sensitivity of the photographic emulsion with electron energy. The method used was essentially that of Slätis,[32] and can give reliable values in most cases. In the study reported herein it was found that the background darkening on the film and the limited energy resolution of the densitometer caused wide disagreement between this method and the other two. For this reason values obtained by Method B were not included in the summary. In cases involving intense lines, values did agree rather well. The L lines of the 126.2-kev transition by this

Table VII

Auger electrons seen in the decay of $Ta^{175}$

| Electron energy (kev) | Relative intensity[a] | Assignment |
|---|---|---|
| 42.61 | W | K $L_I$ $L_I$ |
| 43.14 | MW | K $L_I$ $L_{II}$ |
| 44.34 | W | K $L_I$ $L_{III}$ |
| 44.88 | MW | K $L_{II}$ $L_{III}$ |
| 46.04 | VW | K $L_{III}$ $L_{III}$ |
| 51.51 | VW | K $L_I$ $M_I$ $M_{II}$ |
| 51.72 | VVW | K $L_I$ $M_{III}$ |
| 52.02 | VW | K $L_{II}$ $M_I$ $M_{II}$ |
| 52.48 | VW | K $L_{II}$ $M_{III}$ |
| 53.33 | VVW | K $L_{III}$ $M_{II}$ |
| 53.70 | VW | K $L_I$ $L_{II}$ N |
| 55.26 | VVW | K $L_{III}$ N |

[a] W = weak, M = moderately, V = very.

Table VIII

$Ta^{175}$ Conversion-electron intensity; summary

| Transition energy (kev) | Subshell | Intensity | |
|---|---|---|---|
| | | Visual | Spectrometer |
| 50.5 | $L_I$ | 10.2 | |
| | $L_{II}$ | 9.5 | |
| | $L_{III}$ | 11.5 | |
| 70.5 | $L_I$ | 3.0 | |
| | $L_{II}$ | 7.3 | |
| | $L_{III}$ | 4.5 | |
| 81.6 | $L_I$ | 28 | |
| | $L_{II}$ | 8.8 | 51.3 |
| | $L_{III}$ | 8.7 | |
| 104.3 | K | 40 | 39.4 |
| | $L_I$ | 9.4 | |
| | $L_{II}$ | 2.3 | 10.3 |
| | $L_{III}$ | 1 | |
| 126.2 | K | 20 | |
| | $L_I$ | 2.1 | |
| | $L_{II}$ | 9.3 | 19.7 |
| | $L_{III}$ | 8.0 | |
| 157.1 | K | 1 | |
| 162.5 | K | 9.6 | < 11.7 |
| 179.4 | K | 1.9 | |
| | L | .67 | |
| 186.0 | K | 2.8 | |
| 190.8 | K | 3.0 | |
| 207.9 | K | 4.7 | |
| 267.2 | K | 15 | 14.9 |
| | L | | 2.3 |

method were 19, 4.2, and 9.6, with a total of 19.5, and the K line of the 267.2 transition was 17. Other results were within a factor of 2 of the values in Table VIII.

Method C has the disadvantages of the same large photographic correction factors involved in Method B plus the fact that the comparisons are subjective in nature, depending on the judgement of "lighter" and "darker" by the individual investigator. The method has the great advantage, however, of "subtracting" background by placing the emulsions of the plate and its comparison standard in contact. The surprisingly good agreement between the results obtained by this method and those of Method A indicate that the major uncertainty in the densitometer method is in accurately determining the background darkening of the photographic plate. The L-subshell ratios obtained by Method C are thus expected to be quite reliable. The only area in which accurate determinations could not be made was at low energies below about 35 kev, where the photographic efficiency correction and line shape make any measurement very difficult. The intensity of the 16.19-kev line is not reported in Table VIII since it is not believed to be usefully reliable. The data in Table VIII were normalized so as to give the best average fit between the visual and spectrometric determinations.

## F. $Ta^{175}$ Decay Scheme

Multipolarities of the more intense transitions in the decay of $Ta^{175}$ to levels in $Hf^{175}$ were determined from conversion-coefficient data. The theoretical conversion coefficients used in this study were those calculated by Sliv and Band.[33] Electron screening and finite nuclear size were included in these relativistic calculations. Multipolarity assignments are given in Table IX. The most obvious assignment is for the 126.2-kev transition, where the L-subshell ratio of 1/4.7/3.7 strongly indicates an electric quadrupole case, since for the E2 transitions the $L_I$ conversion coefficient is smaller than that of the $L_{II}$ or $L_{III}$. The observed K/L ratio of 1.0 is a small number, also indicating an E2 transition. The theoretical values are 1/6.1/5.1 and 0.86 for pure E2.

Table IX

$Ta^{175}$ Conversion coefficients and multipolarity assignments

| Transition energy (kev) | Relative electron intensity | Normalized gamma intensity[a] | Multipolarity | α Theoretical | α Observed | K/L Theoretical | K/L Observed | $L_I/L_{II}/L_{III}$ Theoretical | $L_I/L_{II}/L_{III}$ Observed |
|---|---|---|---|---|---|---|---|---|---|
| 50.5 | 31 | | 60% E2<br>40% M1 | 4.9 | | | | 1/.95/1.0 | 1/.90/1.1 |
| 70.5 | 15(L) | | 35% E2<br>65% M1 | 9.1 | | 1.0 | | 1/2.0/1.9 | 1/2.5/1.5 |
| 81.6 | 18(L) | <9 | 7% E2<br>93% M1 | 6.2 | | 3.9 | | 1/.30/.22 | 1/.31/.30 |
| 104.3 | 53 | | 7% E2<br>93% M1 | 3.5 | | 5.2 | 3.8 | 1/.22/.14 | 1/.24/.11 |
| 126.2 | 40 | 29.5 | 94% E2<br>6% M1 | 1.35 | 1.35[a] | 0.99 | 1.0 | 1/4.9/3.9 | 1/4.7/3.7 |
| 162.5 | 12 | 7 | M1 | 1.14 | 1.7 | 7.2 | 8 | | |
| 179.4 | 2.5 | | E2 | 0.36 | | 1.4 | 2.8 | | |
| 207.9 | 5.5 | 25 | M1 | 0.53 | 2.2 | 6.9 | 5-8 | | |
| 267.2 | 17 | 20 | M1 | 0.26 | 0.85 | 7.3 | 6 | | |

a. Gamma intensities normalized to electron intensities to give correct α for the 126.2-kev transition.

Evidently the transition is not pure E2 but has some M1 admixture, and a 94% E2 and 6% M1 photon mixing ratio gives a fit to the experimental data with agreement that is fortuitously good considering the uncertainties in the intensity ratio measurements. Since the fit is very good not only for the triple subshell ratio but also for the K/L ratio, the multipolarity assignment of this transition seems quite certain and its total theoretical conversion coefficient of 1.35 is used as a basis for normalizing the gamma-ray relative intensities to those of the conversion electrons in order to obtain total conversion coefficients for the other transitions. This assumes that the entire 126-kev gamma-ray intensity is due to the 126.2-kev transition. It should be noted that there is an electron line listed in Table V which is assigned as the K line of a 126.7-kev transition whose L lines are not seen. If this is true, then from its intensity one can say that the transition has a high K/L ratio and thus may be electric dipole. If so its gamma intensity is about 50, and thus normalizing in this manner may produce conversion-coefficient values that are low by a factor of as much as 8.5/3. These normalized gamma-ray intensities, given in Table IX, are used in computing total conversion coefficients for the other transitions.

Three of the listed transition multipolarities are very dependent upon the total conversion coefficient. These are of 162.5-, 207.9-, and 267.2-kev energy. In these cases the L-subshell ratios could not be determined and therefore the only other evidence is from K/L intensity ratios. In all three cases the K/L ratio was rather large, being about 8, 5 to 8, and 6 respectively. Table X lists the K/L ratios for these three transitions for different multipolarities.

Table X

Theoretical K/L ratios of some transitions in hafnium

| | Energy (kev) | | |
|---|---|---|---|
| Multipolarity | 162.5 | 207.9 | 267.2 |
| E1 | 6.0 | 6.1 | 6.5 |
| M1 | 7.2 | 6.9 | 7.3 |
| E2 | 1.2 | 1.7 | 2.4 |
| M2 | 3.4 | 4.1 | 4.6 |

From this table it is obvious that the transitions can not be of the quadrupole type, since both E2 and M2 have ratios too low to agree with the experimental values given. This leaves the choice between electric and magnetic dipole. The conversion coefficients are very different for the two, therefore it should be easy to select the correct assignment on this basis provided the gamma-ray intensities have been correctly normalized. The conversion coefficients in question are given in Table XI.

Table XI

Conversion coefficients of some transitions in hafnium

| | Energy (kev) | | |
|---|---|---|---|
| Multipolarity | 162.5 | 207.9 | 267.2 |
| E1 | 0.096 | 0.051 | 0.028 |
| M1 | 1.14 | 0.53 | 0.26 |
| Observed | 1.7 | 2.2 | 0.85 |

The agreement between theoretical and observed values is not very good, but is sufficient to indicate strongly that all three transitions are magnetic dipole. All appear rather high, but the complexity of the gamma-ray spectrum and the question of the pureity of the 126-kev photopeak are expected to produce uncertainty in data such as these which depend upon gamma-ray intensities. Assuming the correction value of 8.5/3 gives much better agreement.

The rather weak transition at 179.4 kev is assigned as E2. The low K/L ratio of 2.8 indicates this assignment, and supporting evidence comes from the fact that neither the $L_I$ nor the $M_I$ line was seen in the conversion-electron spectrum although the $L_{II}$, $L_{III}$, and $M_{II}$ were all easily observed. This indicates a low $L_I/L_{II}$ ratio, which is characteristic of E2 transitions. The theoretical value is 0.35 in this case.

The observed L-subshell ratio of the 81.6-kev transition is 1/0.31/0.30. This agrees reasonably well with the theoretical ratio for an E1 transition of 1/0.35/0.42. If this transition were an E1, however, the gamma-ray intensity would have to be about 550, and the observed

value is less than 9. This assignment is clearly not compatible with that of the 126.2-kev transition. Therefore other possibilities were investigated. The subshell ratios for M1, E2, and M2 are 1/0.095/0.011, 1/18.1/18.1, and 1/0.10/0.27, respectively, and none of these values by itself seems close to the observed one. It is found, however, that a mixture of 7% E2 and 93% M1 gives a value very close to that observed experimentally, as shown in Table IX. It is unfortunate that the K-line energy is too low to give an accurate K/L ratio as further evidence. The theoretical conversion coefficient of this mixed transition is 6.2, which is apparently not in disagreement with the gamma-ray intensity data.

A similar argument to that above may be given for the 104.3-kev transition and the same mixing ratio is found for it as for the one at 81.6 kev. The assignments of the 50.5- and 70.5-kev transitions are based on L-subshell ratios alone, since their photopeaks are buried under the K x-rays in the gamma-ray spectrum and are thus not observed. The mixing ratios observed in this study for the 81.6- and 104.3-kev transitions are very similar to those found in the analogous transitions in the only other 103-neutron isotope known, as is discussed below.

Table XII lists transition-energy sums obtained from the energies determined in conversion-electron studies.

From Table XI it may be seen that the most intense transition is the one at 81.57 kev, and thus one may assume that it proceeds to the ground state. The frist excited state is then at 81.57 kev, and from the first sum in Table XII it is seen that there is a second state at 186.0 kev whose transition to ground is observed in addition to its depopulation to the first excited state by means of the 104.3-kev transition. These data are shown in the proposed decay scheme given in Fig. 12. Two other states may be located on the basis of sums in Table XII at energies of 207.8 and 348.8 kev, since both sum groups include the 81.57-kev ground-state transition.

A double sum without crossover is seen whose energy is 261.4 kev. Only one of its transitions, the one at 104.3-kev, has a known position in the decay scheme. These data may be interpreted as indicating a level at 343.0 kev and another at either 152.1 or 272.4 kev. The situation is

Table XII

| Transition-energy sums in $Ta^{175}$ decay | | |
|---|---|---|
| 81.6 + 104.3 | = | 185.9 |
| Crossover | = | 186.0 |
| 81.6 + 126.2 | = | 207.8 |
| Crossover | = | 207.9 |
| 81.6 + 267.2 | = | 348.8 |
| 140.9 + 207.9 | = | 348.8 |
| 162.5 + 186.0 | = | 348.5 |
| Crossover | = | 349.0 |
| 104.3 + 157.1 | = | 261.4 |
| 70.5 + 190.8 | = | 261.3 |
| 190.8 + 235.6 | = | 426.4 |
| 77.4 + 349.0 | = | 426.4 |
| 70.5 + 186.0 | = | 256.5 |
| 77.4 + 179.4 | = | 256.8 |

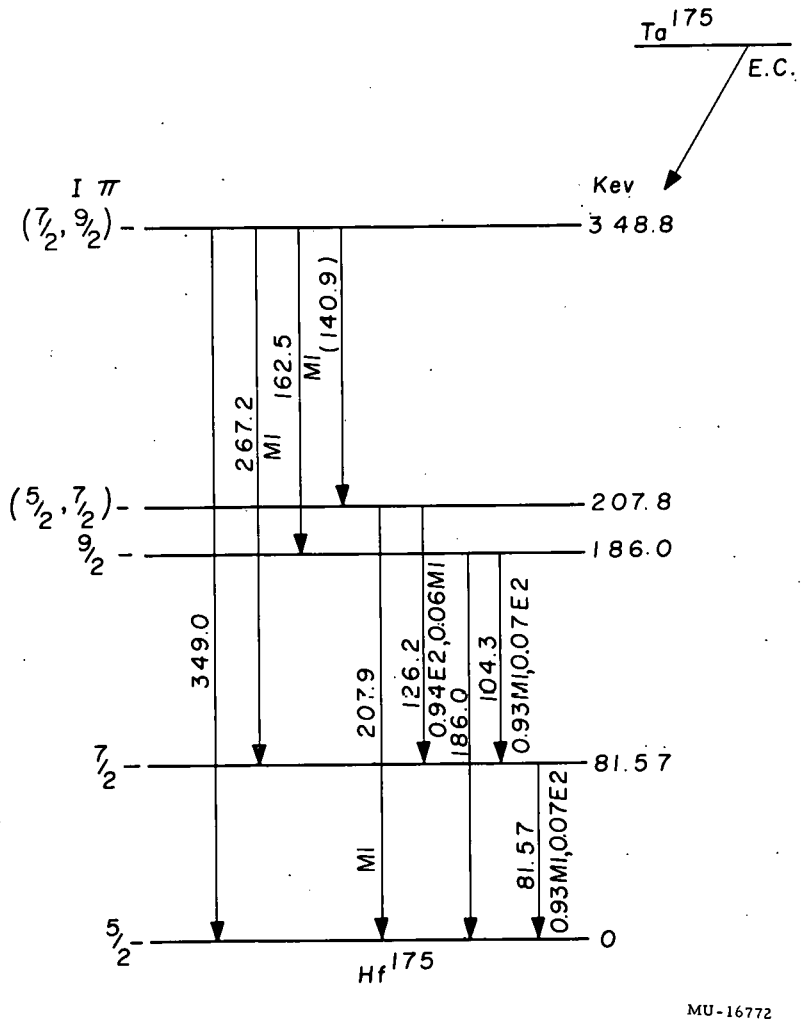


Fig. 12. Proposed partial decay scheme of $Ta^{175}$.

exactly the same for the double sum at 426.4 kev, where in this case a level is indicated at 426.4 kev and either 235.6 or 190.8 kev, with only the position of the 349.0-kev transition being known. Both of these two sum groups use the 190.8-kev transition, and since they cannot both be used in the decay scheme, no decision could be reached as to which, if either, represents the true level sequence. The last sum at 256.5 and 256.8 kev is near the maximum expected error, and since it is not compatible with either of the two previous sums it is believed to be fortuitous.

Eight of the transitions belonging to the decay of $Ta^{175}$ have been established in the decay scheme by the above procedure. In addition to these a weak 75.58-kev electron line is listed in Table VI whose energy is just that expected for the K line of a transition between the 348.8- and 207.8-kev levels, therefore it is thus tentatively assigned.

G. States in $Hf^{175}$

The decay of $Ta^{175}$ takes place to levels in the nuclide $Hf^{175}$, which is composed of 72 protons and 103 neutrons. These numbers are far removed from the regions of closed shells and consequent spherical symmetry. The nucleus is expected to be spheroidal in shape, highly prolate, with a deformation of about $\delta = 0.27$.[22] Low-lying excited states of the rotational type are to be expected whose energy spacings are given to first approximation by

$$E_I = E_0 + \frac{\hbar^2}{2\Im} I(I+1)$$

for states with $K \neq 1/2$. By use of this equation, where $I_0 = 5/2$, and calculating $\Im$ from the energy of the 81.57-kev state, the energy of the 9/2 state is calculated to be 187 kev, in good agreement with the observed value. The energy of the 11/2 state is calculated to be 314 kev.

Intrinsic states in this region may be described in the Nilsson scheme in which they are designated by the quantum numbers $K\ \pi\ (N,n_z,\Lambda)$. Here K is the projection of the total nuclear angular momentum I on the nuclear symmetry axis, $\pi$ is the parity of the state, N is the number of

nodes in the odd-nucleon orbital, $n_z$ is the number of nodal planes perpendicular to the symmetry axis, and $\Lambda$ is the component of the orbital angular momentum of the odd particle along the symmetry axis. Using this notation and the state sequence given by Nilsson as shown in Fig. 13, one notes that the ground state of the 103-neutron nucleus is probably either 5/2- (512) or 7/2- (514). The 105-neutron isotones $Hf^{177}$ and $W^{179}$ have been assigned ground-state spin and parity of 7/2-, and therefore are presumably in the 7/2- (514) state. The only known spin for another 103-neutron isotone is that of $Yb^{173}$, which has been measured as 5/2. It exhibits two excited states at 79 and 180 kev, which are doubtless the 7/2- and 9/2- rotational band members based on the 5/2- ground level, which is almost certainly the 5/2- (512) neutron orbital. This energy spacing is quite similar to that in $Hf^{175}$, and thus the first three levels in Fig. 10 are assigned as the 5/2, 7/2, and 9/2 rotational band levels of the 5/2- (512) state.

Recent publications[34,35] concerning the levels in $Yb^{103}$ list a level at 272 kev which is assigned as the 7/2+ (633) state, previously observed as the ground state of the 107-neutron isotones. The papers also give the mixing ratios for the 9/2 $\longrightarrow$ 7/2 and the 7/2 $\longrightarrow$ 5/2 transitions as 5% E2, 95% M1, which is very similar to the ratios found for transitions between the same states in the $Hf^{175}$ case as discussed previously.

The state at 348.8 kev decays by M1 transitions to the 9/2- and 7/2- states of the ground rotational band, and must thus be of even parity and spin 9/2 or 7/2. The 126.2-kev state decays by a M1 transition to the 5/2- state and partly by M1 to the 7/2- state, and thus must be of odd parity with a spin of 5/2 or 7/2.

Some other interesting comparisons can be made between the experimental results and the predictions of the Bohr-Mottelson model for spheroidally deformed nuclei.[36] The theory allows one to predict the relative intensities of transitions from a common state to different members of a rotational band when the transitions are of the same multipolarity. This may be done for the pairs of M1 transitions at 267.2 and

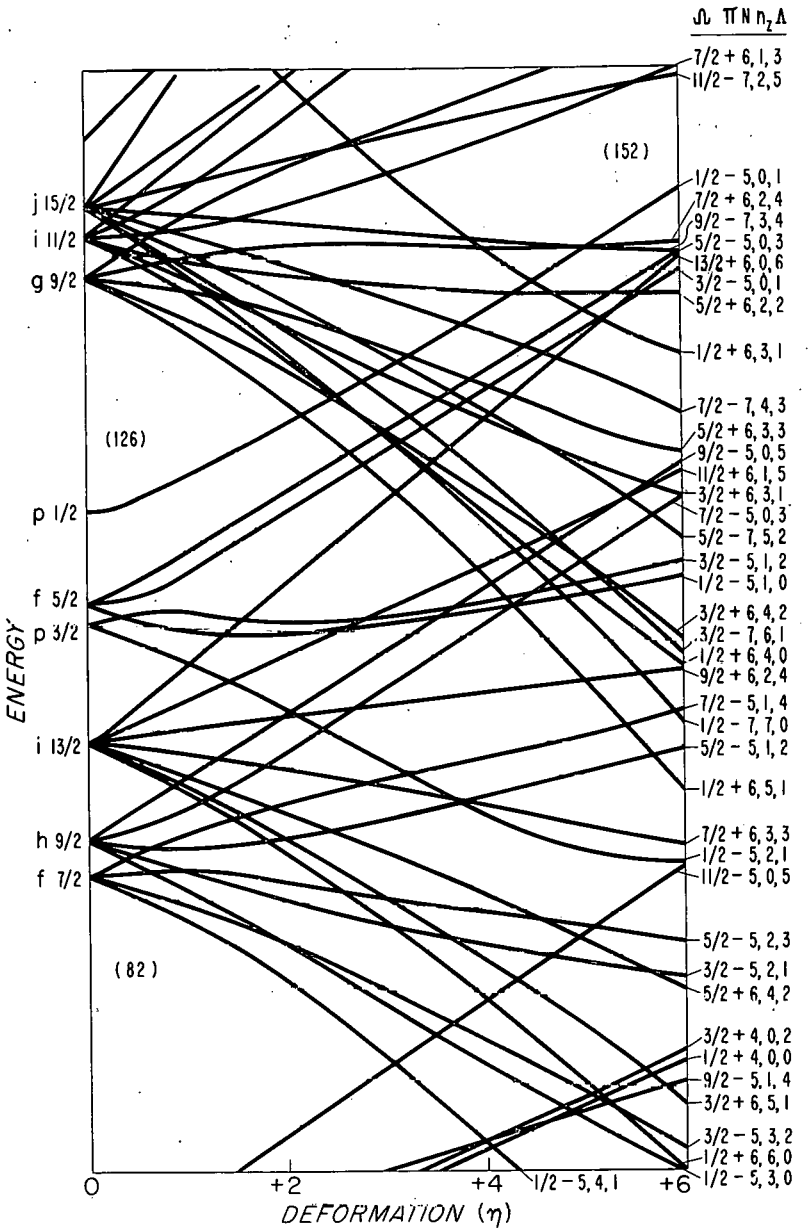


Fig. 13. Nilsson diagram of odd-neutron states in deformed nuclei.

162.5 kev and at 207.8 and 126.2 kev if only the M1 component of the latter is considered. The intensity ratios are proportional to the transition energy to the 2L + 1 power (where L is the transition multipolarity) and the square of the Clebsch-Gordan coefficients between $I_i$ and $I_f$ with K-quantum numbers $K_i$ and $K_f$, i.e.,

$$\langle I_i, L, K_i, K_f - K_i \mid I_f, K_f \rangle .$$

For the first case the energy dependence is

$$\left(\frac{267.2}{162.5}\right)^3 = 4.5 ,$$

and the ratio of the squared Clebsch-Gordan coefficients is

$$\frac{B\,(7/2 \xrightarrow{M1} 7/2)}{B\,(7/2 \xrightarrow{M1} 9/2)} = \frac{\langle 7/2,1,7/2,-1 \mid 7/2,5/2 \rangle^2}{\langle 7/2,1,7/2,-1 \mid 9/2,5/2 \rangle^2} = 8.0,$$

assuming that the initial state is I = 7/2, K = 7/2. If the state is I = 9/2, K = 7/2 the reduced transition probability is

$$\frac{B\,(9/2 \xrightarrow{M1} 7/2)}{B\,(7/2 \xrightarrow{M1} 9/2)} = \frac{\langle 9/2,1,7/2,-1 \mid 7/2,5/2 \rangle^2}{\langle 9/2,1,7/2,-1 \mid 9/2,5/2 \rangle^2} = 1.9,$$

so that the predicted intensity ratio is 1/36 for the 7/2, 9/2- case and 1/8.5 for the 7/2, 7/2- case. The experimental ratio of about 1/3 is much closer to the second case than the first; however, the agreement is not especially good. In this comparison one should remember, however, that either or both transitions may have some E2 admixture and that the limits of error of the experimental ratio are rather large, since the ratio is based on the intensity of the very weak 162.5-kev gamma ray. A small amount of configuration mixing can also alter the predicted ratio rather seriously.

In the case of the 207.8- and 126.2-kev pair, the energy-dependence factor is

$$\left(\frac{207.8}{126.2}\right)^3 = 4.4 .$$

The only state that seems reasonable is the one in which I = 7/2 and K = 7/2, since no K = 3/2 state appears in this region and M1 transitions from a K = 1/2 band are K-forbidden, $\Delta$ K being 2, and thus the Clebsch-Gordan coefficients vanish identically. The reduced transition probability ratios based on states of 3/2, 5/2- and 3/2, 7/2- are 5/2 and 10.2/1 respectively, neither of which give reasonable agreement with experiment. The reduced transition probability for 7/2, 7/2- gives a value of 1/3.4, thus predicting a total intensity ratio of 1/15. The experimental value, assuming 6% M1 for the 7/2- ——> 7/2- transition, is 1/14.

One is tempted from the above calculations to assign the levels as 7/2,9/2- and 7/2,7/2- respectively, but it should be noted that the energy separation of the two is 141.0 kev. The effective moment of inertia parameter $\hbar^2/2\Im$ calculated from this separation is 15.7 kev, while all previously reported values for this state are about 12.6 kev. This plus the fact that the 140.1-kev transition is very weak throws some doubt on the assignments. These effects might be explained by noting that some rotational-band interaction perterbations are to be expected.

Since the M1-E2 mixing ratio of the 7/2- ——> 5/2- intraband transition seems to agree well between the two isotones, it is of interest to calculate what it would be from the theory and compare the results. Bohr and Mottelson[32] give the transition probabilities for E2 and M1 transitions within a rotational band between state I + 1 and I as

$$B(E2) = \frac{5}{16\pi} e^2 Q_o^2 \frac{K^2 (I+1-K)(I+1+K)}{I(I+1)(2I+3)(I+2)}$$

and

$$B(M1) = \frac{3}{4\pi} \left(\frac{e\hbar}{2Mc}\right)^2 \frac{(g_\Omega - g_R)^2 \Omega^2 (I+1-K)(I+1+K)}{(I+1)(2I+3)},$$

where I, $\Omega$, and K are the quantum numbers previously defined, M is the mass of the proton, c is the speed of light, $g_\Omega$ is the gyromagnetic ratio of the last odd particle, $g_R$ that associated with the collective motion of the nucleus, and $Q_o$ the intrinsic quadrupole moment.

A number of the parameters needed in the calculation have been measured for $Yb^{173}$. The spin has been determined as 5/2 by several

investigators,[23,37,38] and the magnetic moment obtained from atomic spectroscopy is given as -0.67[39] and -0.65[37] nuclear magnetons. The published measurements of the quadrupole moment are in wide disagreement, giving $Q_o$ values from 6.7 to 10.9 and therefore were not used. The intrinsic quadrupole moment is given from the theory by

$$Q_o = 0.8\, Z\, R_z^2\, \delta\, (1 - 2/3\, \delta - \cdots),$$

and using values of $\delta = 0.27$[22] and $R_z = 1.2 \times 10^{-13}\, A^{1/3}$ for the nuclear radius gives a value of

$$Q_o \simeq 8.3 \text{ barns}.$$

The factor g is given approximately as

$$g_R \simeq \frac{Z}{A} = 0.41.$$

Bohr and Mottelson[36] give the magnetic moment as

$$\mu = \frac{I_o^2}{I_o + 1}\, g_\Omega + \frac{I_o}{I_o + 1}\, g_R ,$$

where $I_o$ is the ground-state spin. Using the measured value for $I_o$ and the above value for $g_R$, one obtains from this equation a value of

$$g_\Omega = -0.39 .$$

Returning to the equations for the reduced transition probabilities and taking their ratio, one obtains the expression

$$\frac{B\ (E2)}{B\ (M1)} = \frac{5}{4} \left( \frac{\hbar}{2\, Mc} \right)^{-2} \left[ I(I+1) \right]^{-1} \left[ \frac{K}{\Omega}\, \frac{Q_o}{(g_\Omega - g_R)} \right]^2 .$$

Noting that $K = \Omega$ and substituting the values obtained above into this equation, one obtains a mixing ratio of

$$\frac{B\ (E2)}{B\ (M1)} = 2.0 \times 10^{-2},$$

which is to be compared to the 5% or 6% found experimentally. The agreement is quite good considering the approximations involved in obtaining values of $Q_o$ and $g_R$.

# VI. ELECTRON TRACK SPECTROSCOPY

## A. Introduction

The permanent-magnet electron spectrographs are among the more useful and versatile tools available to the nuclear spectroscopist. The accuracy with which transition energies can be determined is second only to such instruments as bent-crystal spectrometers, which are greatly limited by the large amount of activity necessary for their use. The resolution of the spectrographs is about 0.1%, which allows separation of L- and M-subshell lines at energies commonly encountered experimentally. They are relatively inexpensive and are dependable over long periods of time, the only possible breakdown being due to failure of the vacuum system. Their only serious drawback is the difficulty encountered in measuring relative line intensities. It would also be desirable, of course, to retain the above features and still decrease the necessary amount of sample. This investigation was undertaken with both these possibilities for improvement in mind.

As discussed in the section dealing with the conversion-electron spectrum of $Ta^{175}$, the major difficulties encountered in relative-intensity measurements are due to the uncertainties involved in measuring photographic optical density and converting these data into terms of relative numbers of electrons incident upon the photographic plate. Since this problem was previously dealt with in the specific case, the discussion is not repeated here. It is obvious that a method in which individual events are counted -- i.e., an electron striking the photographic plate -- entirely eliminates the problems usually associated with the photographic method.

The technique of counting individual tracks of ionizing particles in photographic emulsions has been used extensively in other fields of investigation. Alpha-particle spectroscopists have developed the method into a widely used technique for the investigation of heavy-element decay schemes. It was felt quite desirable to attempt adaption of the track-counting method to conversion-electron spectroscopy.

Several investigators have published the results of similar studies. Both Antonova[40] and Kleinheins[41] used an electron track method and reported studying the conversion electrons of $Cs^{137}$. Antonova reported an increase in sensitivity for his spectrograph by a factor of 300 to 500 when the counting method was used. These studies were at higher energies than our investigation and magnification was thus less, being from 300 to 450. Kleinheins also investigated the beta spectra of $Co^{60}$ and $Te^{127}$. The instruments in both cases had low resolution and high transmission, the opposite of our case.

A method more analogous to ours was reported by Reitmann et al.[42] in which the lines of the 411.8-kev transition in $Hg^{198}$ were studied by using 100-micron-thick Ilford G5 emulsion at 2000-power magnification.

B. Description of the Method

Standard spectrograph-size plates were obtained with a 25-micron-thick layer of Ilford G5 nuclear emulsion from Ilford Ltd. of England. The plates were stored in the laboratory's underground film-storage cave until needed. Ordinary exposure methods were used in the spectrographs, and development procedures were as described previously in the experimental section.

In order to have plates free from background tracks, a method of background eradication was investigated. Plates were placed inside a stainless steel lighttight tank in an atmosphere saturated with water vapor at 35°C for periods of one to several days. The emulsion softens at these temperatures and the latent images of tracks formed in it are destroyed. There was no noticeable decrease in emulsion sensitivity due to this procedure for treatment periods of up to 3 days. Following a series of tests on background contributions it was found that the amount of background in the plates at the time they were used was negligible compared with the contribution from scattering and contamination within the spectrograph camera, and therefore eradication was not routinely performed.

In addition to the contribution of true electron tracks, there was a decrease in "signal-to-noise" ratio because of spurious developed grains in the emulsion; these are always present, and are a function of development time, development conditions, and other variables. The heaviest concentration of developed grains is at the surface of the emulsion (particularly if the film is not carefully handled, since slight pressure on the emulsion forms some latent image), and two methods were found to eliminate most of these surface grains. First, the addition of ammonium thiosulfate in varying concentrations to the fixing solution seemed to help somewhat, and second, it was found that a damp tissue rubbed gently over the surface of the pellicle could polish away the unwanted layer without affecting the interior of the emulsion. The number of grains remaining inside was still quite large, about $2 \times 10^4$ grains per $mm^2$ in the $Am^{241}$ plate discussed below.

While tracks were being counted the focus depth of the microscope in the emulsion was continuously varied up and down in order to detect tracks that penetrated at steep angles. Some previous investigators have tilted the film with respect to the electron trajectory axis, but this was not done in this study. Because the paths of the electrons in the medium were very crooked it was not considered to be of significant benefit, and furthermore would have added a complication in line shape and position. The actual thickness of the emulsion layer could be increased by soaking the plate in glycerine prior to counting if desired.

Of critical importance to the usefulness of a counting method are the track length and grain spacing of the track. Grain spacing is of interest since it becomes increasingly difficult to recognize tracks when the mean distance between the grains in a track approaches the mean random grain spacing. Zajac and Ross[43] reported a study of mean range and number of grains developed per track in a similar emulsion, Kodak NT4. Their electron energies varied from 30 to 250 kev and the results seem in good agreement with out observations on Ilford G5. Some of their data are shown in Table XIII.

Table XIII

Electron ranges and numbers of grains per track in photographic electron emulsion

| Electron energy (kev) | Mean range (microns) | Mean No. of grains per track |
|---|---|---|
| 30 | 7.0 ± 0.3 | 11.0 |
| 40 | 10.8 ± 0.4 | 13.8 |
| 50 | 15.8 ± 0.5 | 20.4 |
| 60 | 21.4 ± 0.6 | 22.4 |
| 80 | 32.7 ± 1.6 | 35.5 |
| 100 | 46.7 ± 1.5 | 43.3 |
| 147 | 95.4 ± 1.2 | 74.2 |
| 200 | 141 ± 6 | 95 |
| 250 | 201 ± 8 | 133 |

From these one can calculate the grain density along a track, and the results are shown in Fig. 14. It is seen that the track density through this energy region is not changing very rapidly, so that it should be possible to extend the method to a few hundred kev by suitable variation in the degree of magnification of the counting microscope. In order to record all or most of the track it would ne necessary, however, to increase the emulsion thickness for electrons of higher energy. So far our investigations have been with the thin emulsions in the low-energy region.

Figures 15, 16, and 17 are photomicrographs of electron tracks in a typical plate. This plate is from a short exposure to an $Am^{241}$ source. Magnification is about 1000 x. Figure 15 shows an area of high track density near the maximum of the $L_I$ line of the 59.6-kev transition. The energy of the incident electrons is about 38 kev and the track lengths are about 10 microns, in agreement with the data of Table XIII. In area 1 the individual track locations have been drawn in. Onc notes that most of the tracks in this area can be recognized with this single depth setting; however, the dark spots numbered 4, 5, 6, and 7 are typical

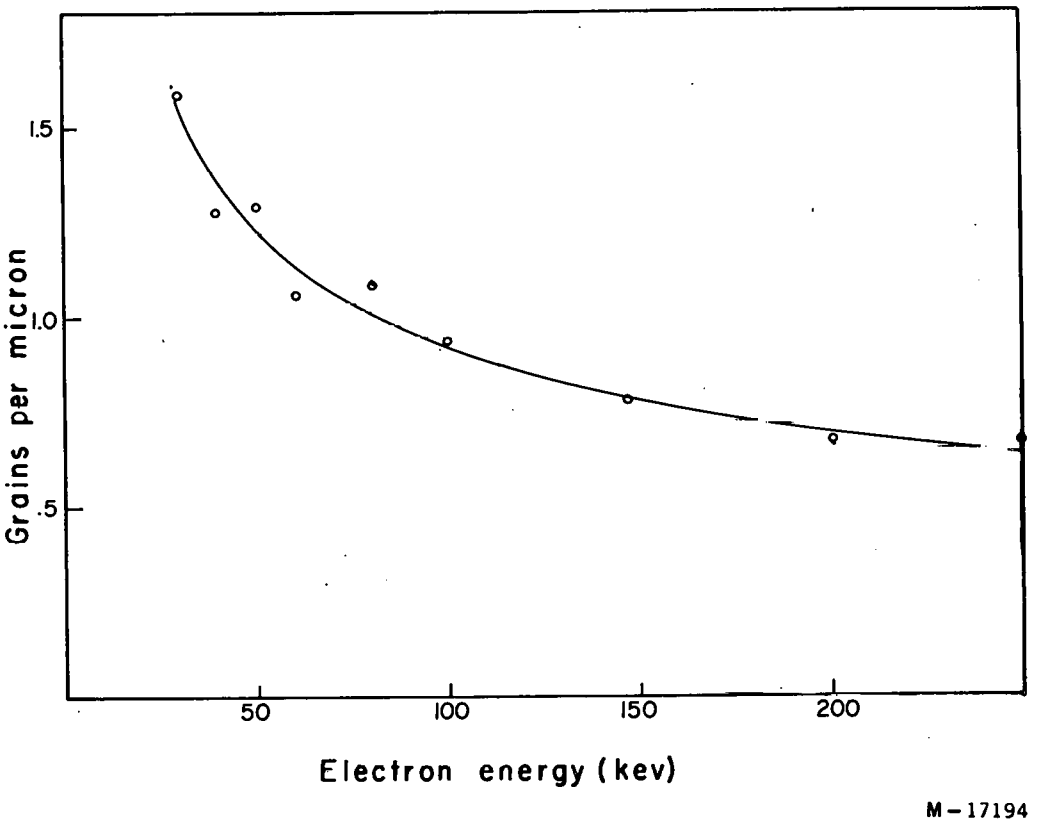


Fig. 14. Grain spacing in electron-track nuclear photographic emulsion.

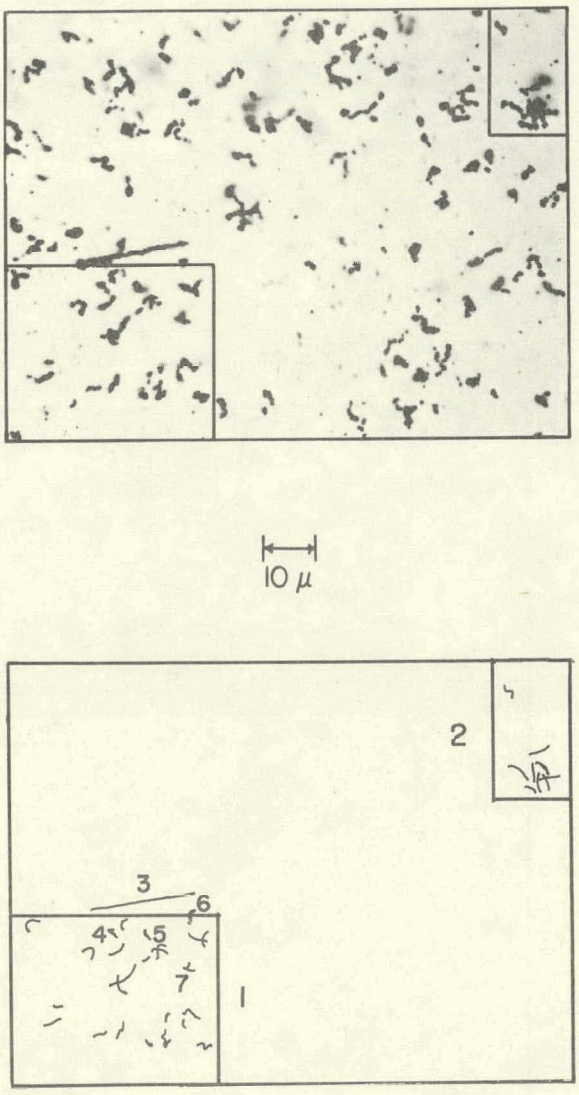


MU-17202

Fig. 15. Photomicrograph of electron tracks in a region of high track density.

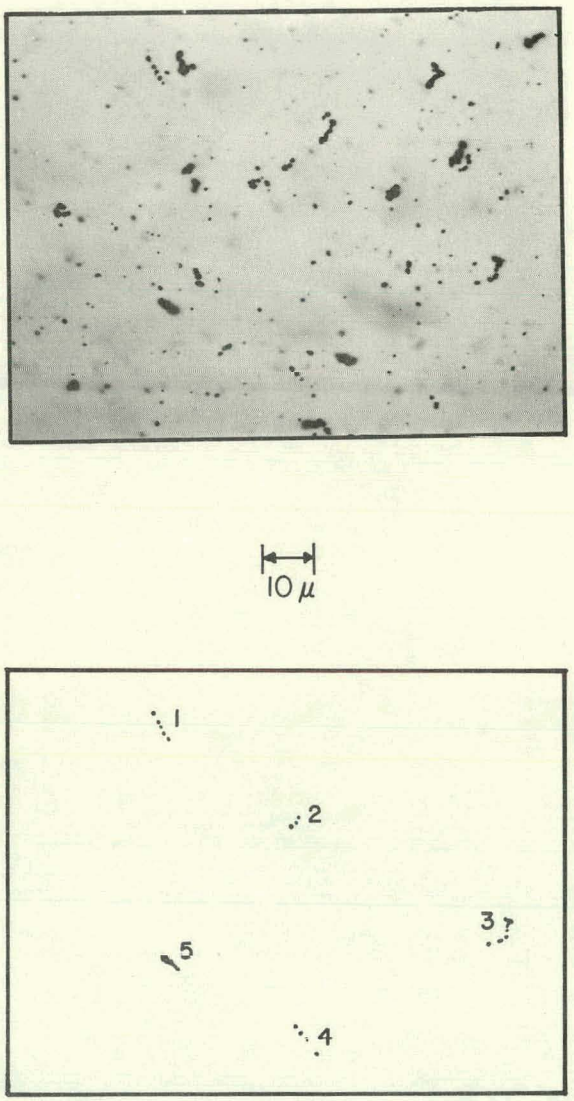


Fig. 16. Photomicrograph of electron tracks in a region of moderate track density.

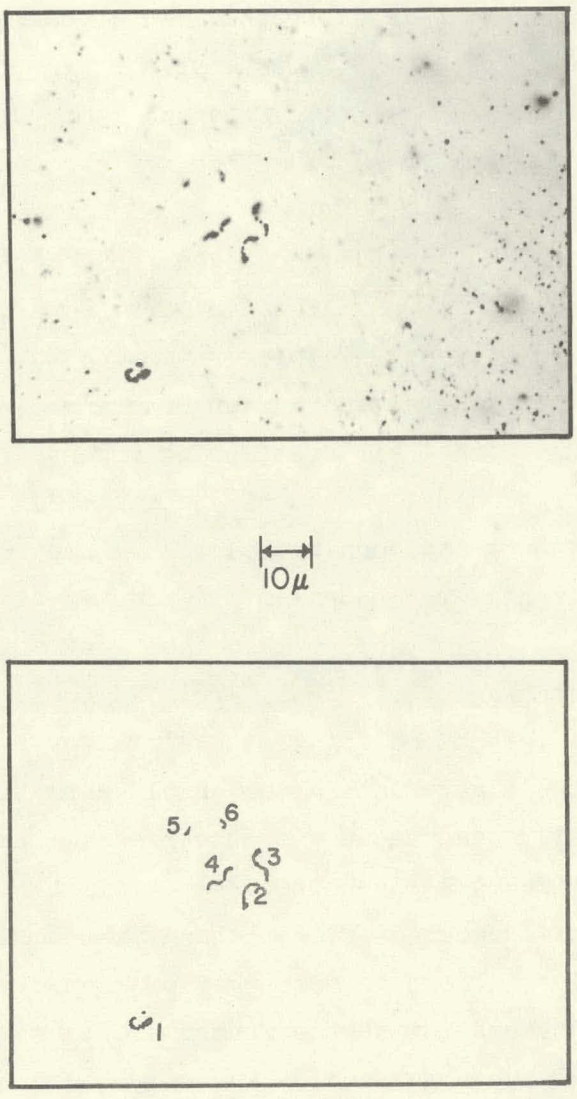


MU-17200

Fig. 17. Photomicrograph of electron tracks in a line-free background region.

examples of darkened areas not recognizable as tracks. By moving the focus-depth setting of the microscope up and down it is easy to decide if they are random spots or tracks, since the latter are seen to have extensive depth into the film so that a short portion of the track is in focus for several microns. Provided there is little overlapping, a continuous slight up-and-down motion while counting makes it very easy to distinguish tracks.

Area 2 in Fig. 15 shows the probable location of the individual tracks giving rise to an extensive darkened area. This area would be partly resolved by vertical-focus variation but there would still be some uncertainty as to the actual number of tracks in the group. The presence of such groups, with their overlapping tracks, indicates the approach to the maximum track density that can be counted. It has been found that the maximum number that can be counted without appreciable uncertainty is about $10^4$ tracks per square millimeter of plate surface, for electrons of this energy. It may be noticed that most of the spurious "fog" grains in this figure are out of focus. This is because focus is rather deep in this photomicrograph and fog grains are almost always near the surface. Number 3 in the figure designates an alpha-particle track. These tracks are occasionally seen because of the presence in the spectrograph cameras of contamination by alpha-particle-emitting isotopes from previous samples, and perhaps also because of scattering from the source itself if it emits alpha particles. There is no danger of mistaking the alpha-particle tracks for electron tracks, since the former are long, dense, and very straight compared with electron tracks. The only undertainty is due to the alpha-particle tracks crossing electron tracks in a small angle, thus causing electrons to be overlooked in the count. This particular alpha-particle track is seen to cross at least one electron track.

Figure 16 is a photomicrograph taken in an area of lower-track-density in the low-energy tail of the conversion-electron line. There are roughly 15 tracks in the figure from electrons of about the right energy. In addition, at the positions labeled 1, 2, 3, and 4 one sees tracks whose grain spacing is too wide to be attributed to electrons of 40 kev energy. These are probably all high-energy Compton electrons and

photoelectrons produced in the camera by the gamma radiation from the sample. On the basis of grain spacing one may discriminate against the high-energy electrons striking the plate. One may discriminate against low-energy ones resulting from electron scattering by their short length and dense grain spacing. This is an advantage of the method; it is almost unique to track counting. In addition to these events there is a track at position 5 which is undoubtedly an alpha-particle track, and this can be easily seen by varying the vertical focus, since it would appear as a long, straight and very dense line.

An area at a higher-energy spectrograph plate setting where the background is very low may be seen in Fig. 17. Tracks labeled 1, 2, and 3 are easily recognized as due to single electrons. Numbers 5 and 6 are probably tracks of low-energy scattered electrons. Number 4 may be either two tracks, each partly out of focus, or a single track with a sharp collision angle. The question could be easily decided by changing the vertical focus. This would probably not be necessary in practice, since the region of the emulsion that appears in focus on the photomicrograph is significantly less than that in focus visually when one is counting. It should be mentioned also that the photomicrograph equipment produced magnification only 70% that of the counting microscope used in collecting the data presented below. The 6-by-6-square grid reticle was not reproduced in the photographs, either. This grid is a great help in actual counting, since the counting area was thus conveniently divided into smaller areas which allowed one to make a count in a series of six horizontal or vertical sweeps of the eye for a single microscope stage setting.

Two different magnification strengths were used in this study. The 12 x eyepieces were used in conjunction with a 90 x oil-immersion objective to give a field of view similar to that seen in the photomicrographs, and also in conjunction with a 43 x dry objective. These arrangements will be referred to as "high" and "low" power respectively.

The counting area under high power was a square 85.7 microns by 85.7 microns divided into 36 equal smaller squares. When counting through a given region, one took counts each 100 microns, and thus there

was no overlap. When an area known to contain a peak was being counted the stage setting was made every 50 microns in order to obtain more closely spaced points. The extent of overlap is shown in Fig. 18 along with the counting areas under low-power magnification. When low power was used the counting field was 168 by 168 microns square, giving a total area of 0.0282 $mm^2$. Stage settings were made at 200-micron intervals when this magnification was used, except that in known peak areas settings were reduced to 100 microns. Alternately, at low power, the field was counted as six vertical strips to decrease the point spacing. A discussion of the relative advantages of each method appears in the following section dealing with experimental results.

C. L-Subshell Ratios at 30 kev

One of the samples selected for testing the electron track method was $Am^{241}$. This isotope populates levels in $Np^{237}$ by alpha decay, and the subsequent gamma-ray transitions include one of 59.6 kev. The energies of the L-subshell conversion-electron lines are 37.2, 38.0, and 42.0 kev, and the relative-intensity ratio of the three lines has been well studied. Table XIV summarizes the results given by some of the investigators who have determined this ratio.

Table XIV

59.6-kev $Np^{237}$ L-shell conversion-electron intensities

| Reference | Relative Intensities | | |
|---|---|---|---|
| | $L_I$ | $L_{II}$ | $L_{III}$ |
| 44 | 1 | 1.9 | 0.59 |
| 45 | 1 | 2.0 | 0.42 |
| 46 | 1 | 2.1 | 0.45 |
| 47 | 1 | 2.2 | 0.67 |
| 48 | 1 | 2.0 | 0.62 |

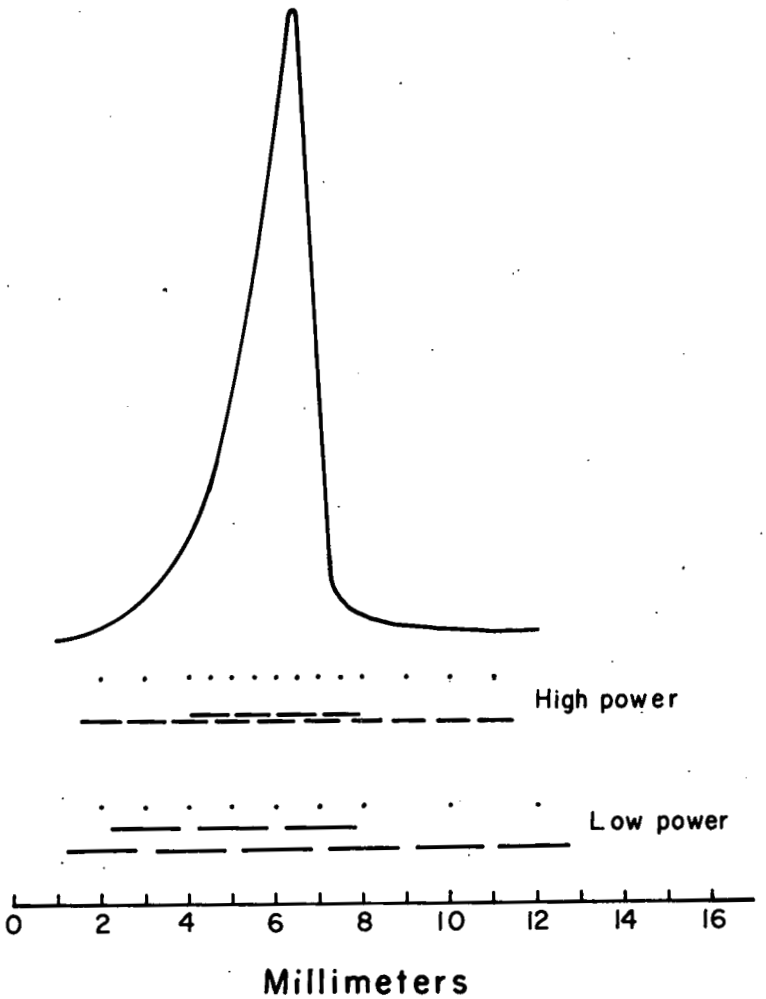


Fig. 18. Diagram of counting fields used under high- and low-power magnification, showing variation used in the region of a suspected line.

In our investigation a strong $Am^{241}$ source was recorded on the 99-gauss spectrograph for 1 day. The resulting plate showed the $L_I$ and $L_{III}$ lines as just barely visible, the $L_{II}$ being rather easily seen. An exposure of the same length of time using the same source with Kodak Noscreen x-ray film, which is routinely used in the spectrographs, gave nearly identical visual darkening. This indicates similar optical sensitivity of the two films to electrons of this energy. The entire area of the three lines was counted under high magnification four times at different vertical stage settings. The number of tracks at each horizontal position was summed for each setting and the results were plotted as number of tracks counted in the four scans, versus distance along the plate (in millimeters). This curve is seen in Fig. 19. Limits of error are not given, since the standard deviation due to the number of tracks counted is obvious and the contribution from uncertainties in track recognition is difficult to estimate.

The maximum number of counts shown is 310, which represents about 80 tracks per field of view. This is very close to the maximum electron-track density that can be counted at this magnification. The background counts in the area around 6 mm on the scale shown is about 25 electrons. The maximum signal-to-noise ratio that one can obtain under these conditions is thus about 12. The peak at 7.5 mm is easily seen even at these rather low counting statistics, and it has a ratio of less than 2. The shape of the peak can presumably be improved significantly by more counts, thus decreasing the uncertainty due to statistical fluctuations. A number of lines are seen between the $L_{II}$ and $L_{III}$ lines, and one between the $L_I$ and $L_{II}$. These are all known lines and groups of lines from other transitions in $Np^{237}$. The peak at 7.5 mm is assigned as the sum of the M lines of a transition at 43.5 kev.

The relative intensities of the three conversion-electron lines may be obtained by taking a ratio of the areas of their peaks corrected for differences in spectrograph geometry. This procedure results in a ratio of $L_I/L_{II}/L_{III} = 1.0/2.1/0.50$, in good agreement with the other

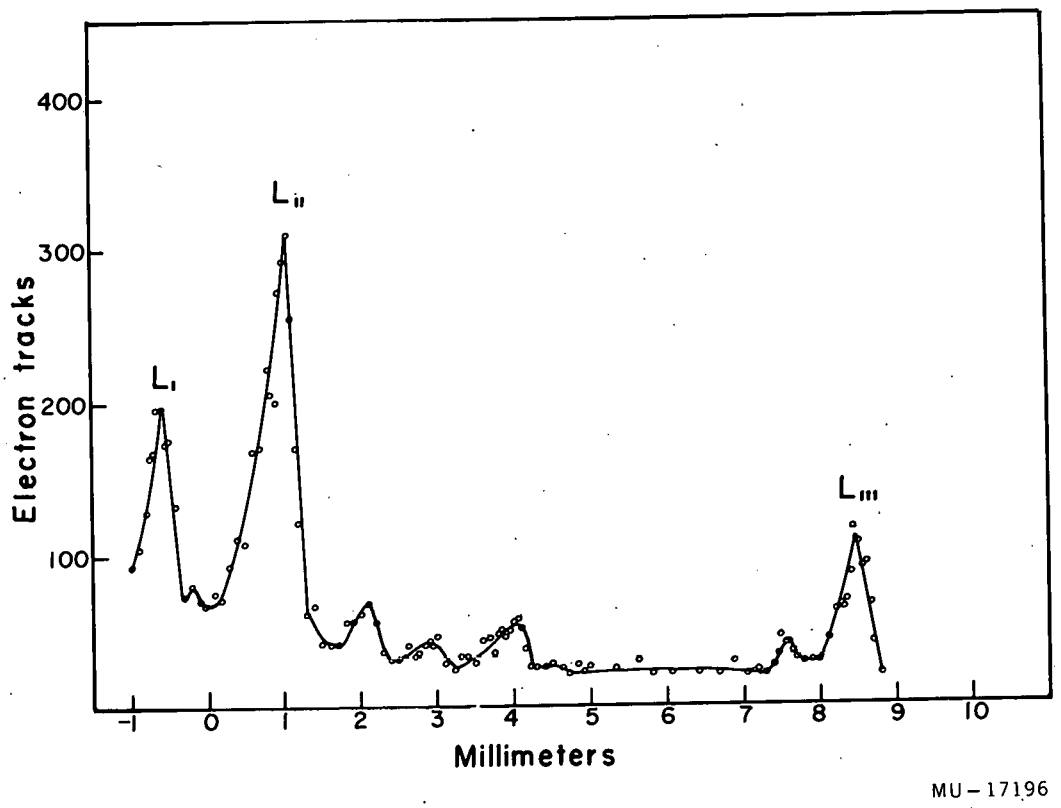


Fig. 19. Track density of the 59.6-kev transition L-subshell lines in $Np^{237}$ counted under high-power magnification.

values in Table XIV. In this table one notes that all values of $L_I/L_{II}$ are in excellent agreement. The variation in the relative intensity of the $L_{III}$ line is partly due to its smaller value and consequent greater uncertainty, and also due in part to the fact that in most intensity-measurement methods the weak line on its low-energy side would not be resolved out but would be included in the reported intensity of the line. Thus the reported values for the $L_{III}$ line are expected to vary with the resolution of the instrument used in its determination. This is verified by the fact that our value of 0.50, in which the line is completely resolved, is among the lower ones reported.

The same spectrograph plate was also counted at low magnification. Only two counting areas per stage setting were counted, as opposed to four areas under high magnification. The larger counting area allowed a maximum of 575 tracks to be counted in this method compared with only 310 for the previous one, even with half the number of counts being made. This gives a calculated counting-area ratio of 3.71, while the measured area ratio is 3.83. The difference is well within the limits of error in the field measurement and counting statistics, indicating that the same numbers of electrons were counted per unit area with both magnifications. The signal-to-noise ratio has a maximum value of 6.7 at this magnification, reflecting the greater difficulty in distinguishing between tracks of the correct energy and scattered electron tracks. The curve in Fig. 20 also demonstrates the loss of resolution with lower magnification.

D. Higher-Energy Conversion-Electron Lines

In order to explore the sensitivity of the method and to look at tracks of higher-energy electrons, a sample of $Pa^{233}$ was investigated on a 160-gauss spectrograph. The lines chosen to count were the 198-kev K line and the 291-kev L lines of the 313-kev transition, and the 280-kev L lines of the 301-kev transition. These lines are shown in Figs. 21 and 22. Three counting areas per microscope stage setting were scanned. Since areas of different dimensions were experimented with during these

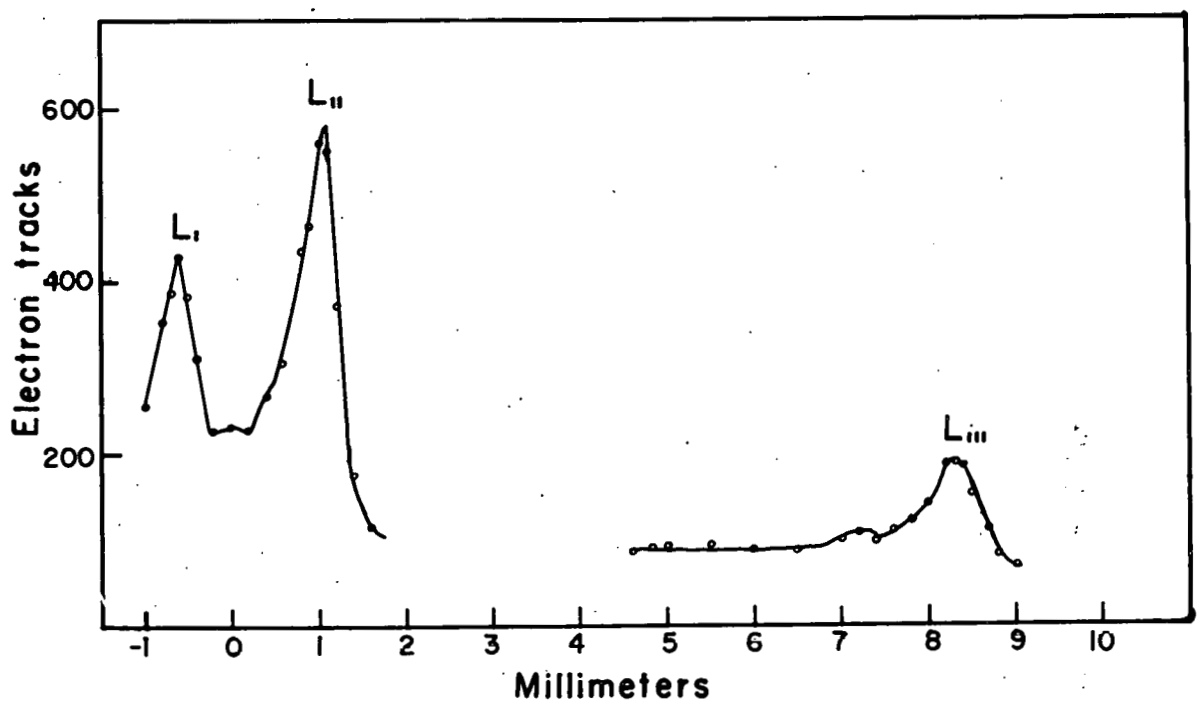


MU-17197

Fig. 20. Track density of the 59.6-kev transition L-subshell lines in $Np^{237}$ counted under low-power magnification.

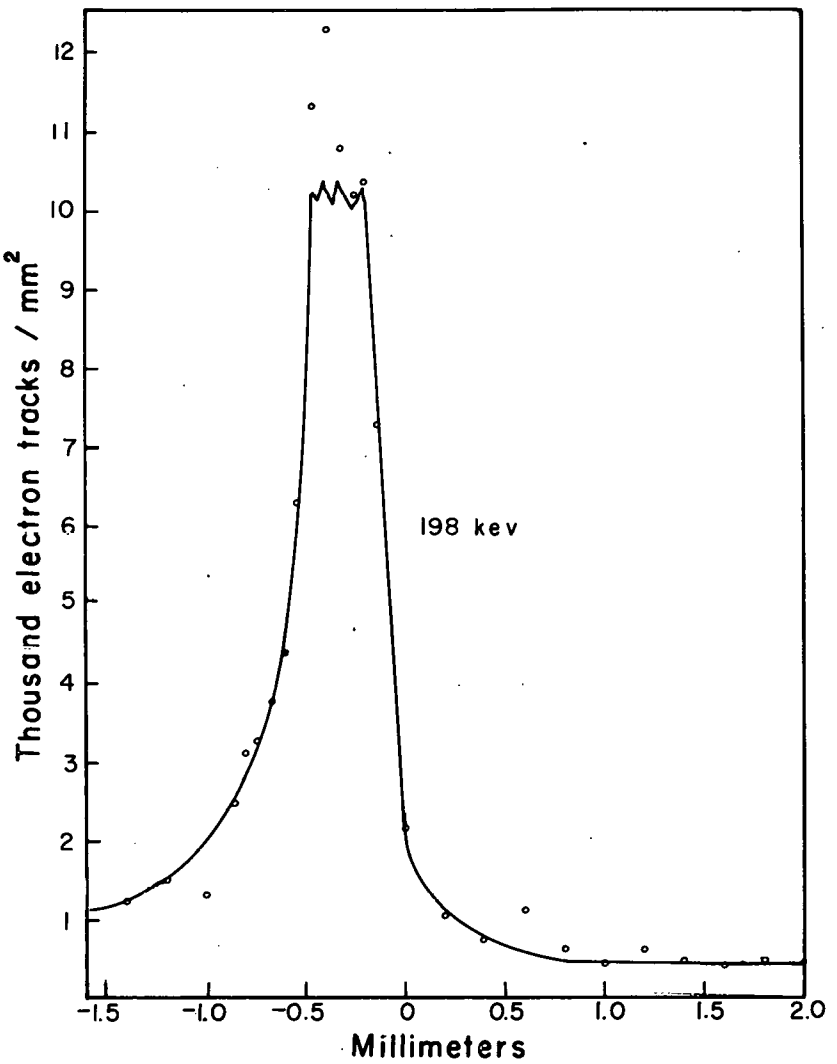


Fig. 21. 198-kev conversion-electron line in the decay of $Pa^{233}$.

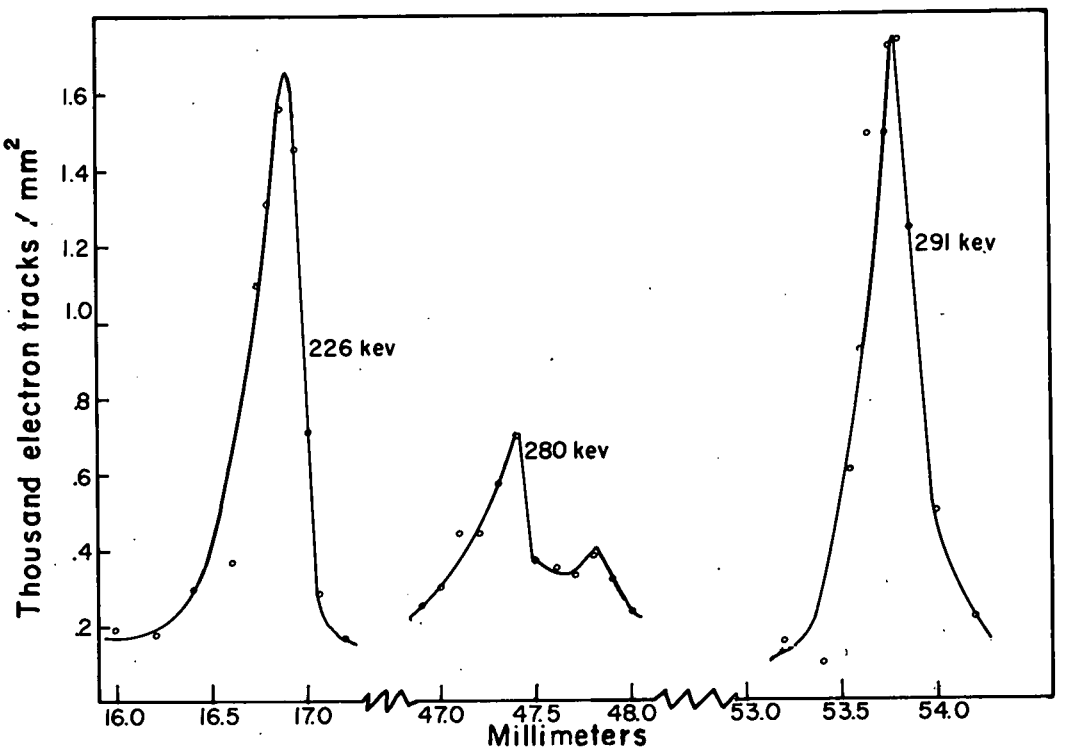


Fig. 22. Conversion-electron lines in the decay of $Pa^{233}$.

counts, the results are normalized to give the numbers of electron tracks per square millimeter. All counting was done under low-power magnification. Exposure time was 15 minutes.

The 198-kev line was easily visible. It may be seen in Fig. 23, where the track plate that was counted in this experiment is compared with a plate exposed on the same spectrograph for a longer period of time. The lines are all easily seen in the latter plate. Only those sections of the plates are shown in which the lines appear. The lines at 226 and 291 kev can just be seen in the track plate under good conditions, but the lines at 280 kev are not visible.

Figure 21 shows the results for the 198-kev line, which is the most intense line in the $Pa^{233}$ spectrum. It was immediately obvious to the investigator that in the area of greatest track density the number of tracks could not be accurately counted because of great uncertainty in resolving separate tracks. This fact is definitely seen in the figure, since all counts above 7,500 tracks per $mm^2$ are random and obviously low. This again indicates an upper limit of about $10^4$ tracks per $mm^2$ as the maximum countable track density. The maximum signal-to-noise ratio is apparently near 12 or slightly higher. Since the spectrometer used for this sample was new and relatively free from contamination, and since the exposure time was shorter by a factor of 96, it is believed that most of the background comes from electrons scattered from the source and not from camera contamination.

The density of tracks necessary to give a visible line can be seen from Figs. 22 and 23. The 291 kev line is visible and the 226-kev line is just at the lower limit of visibility. This indicates that a density of about 1,500 tracks per $mm^2$ makes the line visible at this energy. It is also noted that the presence of a line whose maximum track density is around 400 is easily confirmed by this method.

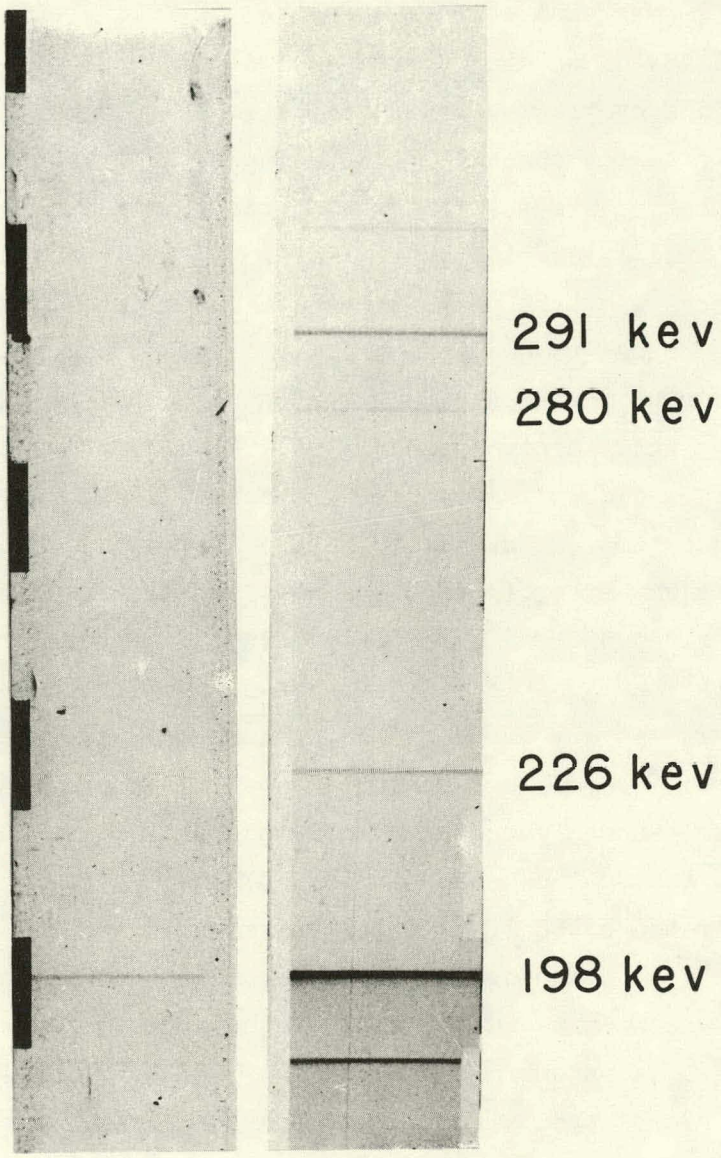


ZN-2134

Fig. 23. Sections of the electron-track plate of $Pa^{233}$ used in this study and a standard plate exposed for a much greater length of time on which all lines are easily visible.

E. Discussion

One of the objectives of this study was to determine the feasibility of obtaining accurate relative intensities of conversion-electron lines by track counting. The good agreement between the value obtained for the L-subshell ratio in the $Np^{237}$ transition and values reported by others shows that the method can give reliable results. The labor involved is considerably greater than for other methods. The time necessary to obtain the data on the $Np^{237}$ transition was several hours. This is offset to some extent by the greater accuracy possible. First, the resolution of the spectrograph can be fully utilized as an aid in avoiding uncertainty caused by contributions to observed intensities from other close lines. This was seen clearly in the $L_{III}$ line in the $Np^{237}$ transition. The second factor is that one can, by repeated counting over a given area, improve the statistical certainty of the results to any desired degree. Third, the great uncertainty due to mathematical conversion of optical density to number of electrons is entirely removed. This is very important when lines are widely separated in energy. The fourth possible advantage comes from the fact that lines are countable even though they are very much less intense than is usually necessary, so that ratios can still be obtained although the amount of exposure is limited by short half life or small amount of activity.

The second possible usefulness of the method was to increase the effective sensitivity of the spectrographs. The increase actually seen is rather disappointing. All three lines in the $Np^{237}$ transition could be seen visually and the other lines seen in the area become obvious only after repeated counting. These lines would probably not have been seen in a single count through the studied film area if they had contained less than 50 tracks on the scale used in Fig. 19. Since a line needed only about 100 tracks to be visible, the sensitivity increase at 30 kev is a factor of only about 2. It should be further noted that the area counted was about 1/2 inch out of a total of 15 inches of the spectrograph plate. The labor involved in counting an entire plate is obviously prohibitive for most cases, and restricts the method to searching an

area in which one has reason to expect the occurrence of lines. Of course, this is usually the case, since gamma-ray spectra can be obtained on samples of limited size, and conversion-electron energies may be estimated from them.

The increased sensitivity is rather better at higher energies. From Fig. 22 one sees that the track density of 1,500 per $mm^2$ is just visible, and the line of only 400 per $mm^2$ is easily located. This indicates an increase in sensitivity by a factor of about 4.

In comparing the two degrees of magnification used, it is noted that at low power one can count much larger numbers of tracks per stage setting and thus per unit time. The disadvantages are in decreased signal-to-noise ratio because of loss of discrimination ability and decreased resolution. A combination of the two might be used where a low-power scan determines the position of lines and a high-power count confirms them and measures relative intensities.

Of general interest to those who use these spectrographs is the number of electrons needed to produce a visible line on the spectrograph plate. Since the lines are about 15 mm long, the number needed at 30 kev, deduced from the $Am^{241}$ sample, is about 13,500 electrons per line. A similar calculation at 250 kev for $Pa^{233}$ gives a value of about 12,000 electrons per line. Also of interest is the fact that even near 300 kev the paths of the electrons in the emulsions are such that most of their energy is degraded within the emulsion layer.

In summary, the method seems useful in cases involving limited activity where an increase in sensitivity by a factor of 2 to 4 justifies the time necessary to count the plate, or where complexity of the spectrum demands maximum energy resolution. The ideal sample should have a low beta background and the energy of the lines should be a few hundred kev or less with present emulsion thickness and degree of magnification.

Acknowledgments

I wish to express my sincere gratitude for the encouragement and guidance of Professor John Rasmussen, under whose direction this work was made possible.

Special thanks are due to Dr. Jack Hollander, who guided the initial phases of my work here; Dr. Kenneth Toth, who suggested the experiment to confirm the mass assignment of $Tb^{152}$; and to Dr. Donald Strominger for performing the electronic measurement of the state half lives in $Dy^{161}$ on his equipment as well as for many helpful discussions.

The crews of the 60-inch cyclotron and the heavy-ion linear accelerator have been most helpful.

Thanks are expresses to the Health Chemistry group for arranging irradiations at the Materials Testing Reactor as well as for handling and monitoring the targets from all bombardments.

Thanks are also in order to John Unik, Glen Gordon, Tom Marshall, Roy Albridge, Jim Schooley, Jim Haag, and other fellow students without whose stimulating and diverting conversations this work might have been completed rather earlier -- but only at the cost of a possible lapse of my interest in the fields of political science and philosophy.

This work was performed under the auspices of the United States Atomic Energy Commission.

List of Tables

List of Figures

REFERENCES

1. Thompson, Harvey, Choppin, and Seaborg, J. Am. Chem. Soc. 76, 6229 (1954).

2. Stevenson and Hicks, Separation of Tantalum and Niobium by Solvent Extraction, UCRL-2009, November 1952.

3. B. G. Harvey (UCRL), unpublished data.

4. W. G. Smith and J. M. Hollander, Phys. Rev. 101, 746 (1956).

5. "Penco" Analyzer manufactured by Pacific Electronuclear Company, Culver City, California.

6. J. O. Juliano, Coincidence Nuclear Spectrometry with Applications to Europium-154 and Europium-155 (thesis), UCRL-3733, April 1957.

7. Ghiorso and Larsh, in Chemistry Division Quarterly Report, UCRL-2647, July 1954.

8. G. D. O'Kelley, The Spectrometric Determination of Some Beta-Particle and Conversion-Electron Energies (thesis), UCRL-1243, June 1951.

9. R. L. Heath, Scintillation Spectrometry Gamma-Ray Spectrum Catalogue, IDO-16408, July 1957.

10. P. Axel, Rev. Sci. Instr. 25, 391 (1954).

11. R. G. Albridge, Jr., I. Nuclear Spectroscopic Studies in the Heaviest Element Region. II. An Electron-Accelerating Spectrograph (thesis), UCRL-8642, 1959.

12. Handley, and Lyon, Phys. Rev. 99, 1415 (1955).

13. K. S. Toth, Nuclear Studies in the Rare Earth Region (thesis), UCRL-8192, March 1958.

14. Mihelich, Harmatz, and Handley, Phys. Rev. 108, 989 (1957).

15. Toth and Rasmussen, Nuclear Spectroscopic Studies of Neutron-Deficient Isotopes in the Rare Earth Region, Phys. Rev. (to be published).

16. Strominger, Hollander, and Seaborg, Revs. Modern Phys. 30, 585 (1958).

17. Cork, Brice, Schmid, and Helmer, Phys. Rev. 104, 481 (1956).

18. Smith, Hamilton, Robinson, and Langer, Phys. Rev. 104, 1020 (1956).

19. S. A. Moszkowski, in Beta and Gamma Ray Spectroscopy, K. Siegbahn Ed., (North-Holland Pub. Co., Amsterdam, 1955).

20. C. W. McCutchen, Phys. Rev. 109, 1211 (1957).

21. D. R. Bès, Nuclear Phys. 6, 645 (1958).

22. Mottelson and Nilsson, Kgl. Danske Videnskab. Selskab. Mat.-fys. Skr. 1, No. 8 (1959); and S. G. Nilsson, Kgl. Danske Videnskab. Selskab Mat.-fys. Medd. 29, No. 16 (1955).

23. Cooke and Park, Proc. Phys. Soc. A69, 282 (1956).

24. Hansen, Nathan, Nielsen, and Sheline, Nuclear Phys. 6, 630 (1958).

25. Baranov, Rodionov, Shishkin, and Chistiakov, J. Exptl. Theoret. Phys. (U.S.S.R.) 37, 946 (1958).

26. Nilsson and Rasmussen, Nuclear Phys. 5, 617 (1958).

27. A. G. W. Cameron, A Revised Semi-Empirical Atomic Mass Formula, Atomic Energy of Canada Limited Report 433, CRP-690.

28. Keepin, Wimelit, and Zeigler, J. Nuclear Energy 6, 1 (1957).

29. Feenberg and Trigg, Revs. Mod. Phys. 22, 399 (1950).

30. F. F. Flebcr, Jr., Nuclear Decay Schemes of Some of the Isotopes of Tantalum (thesis), UCRL-3618, January 1957.

31. Marmier and Boehm, Phys. Rev. 97, 103 (1955).

32. H. Slätis, Arkiv Fysik 8, 441 (1954).

33. Sliv and Band, Coefficients of Internal Conversion of Gamma Radiation, [Acad. of Sciences, U.S.S.R. (1956)]. Translation issued in the United States as Reports 57, ICCKI (1956) and 58, ICCLI (1958), University of Illinois, Urbana, Illinois.

34. Bobrov, Gromov, Dzhelepov, and Preobrazhenskii, Bull. Acad. Sci. U.R.S.S. 21, 942 (1957).

35. Grodinskii, Murin, Pojrovskii, and Preobrazhenskii, Bull. Acad. Sci. U.R.S.S. 21, 1005 (1957).

36. Bohr and Mottelson, Kgl. Danske Videnskab Selskab, Mat.-fys. Medd 27, No. 16 (1953).

37. J. E. Mack, Revs. Modern Phys. 22, 64 (1950).

38. Krebs and Nelkowski, Ann. Physik 15, 124 (1954)

39. Krebs and Nelkowski, Z. Physik 141, 254 (1955).

40. I. A. Antonova, J. Exptl. Theoret. Phys. (U.S.S.R.) 30, 571 (1956).

41. P. Kleinheins, Z. Naturforschg. 11, 252 (1956).

42. Reitmann, Schneider, and von Heerden, Phys. Rev. 110, 1093 (1958).

43. Zajac and Ross, Nature 164, 311 (1949).

44. Rosenblum, Valadares, and Milsted, J. phys. radium 18, 609 (1957).

45. F. L. Canavan, University of California Radiation Laboratory, unpublished results, February 1956.

46. Baranov and Shliagin, Conf. Acad. Sci. U.S.S.R. on Peaceful Uses of Atomic Energy, Phys. Math. Sci., p. 251 (July 1955); Consultants Bureau Translation, p. 183.

47. Hollander, Smith, and Rasmussen, Phys. Rev. 102, 1372 (1956).

48. Rasmussen, Canavan, and Hollander, Phys. Rev. 107, 141 (1957).